Turkish Journal of Earth Sciences (Turkish J. Earth Sci.), Vol. 20, 2011, pp. 321–335 . Copyright ©TÜBİTAK
doi:10.3906/yer-0904-4 First published online 25 October 2010

Late-medieval plagioclase-titanaugite-bearing Iron Slags of the Yapraklı Area (Çankırı), Turkey

W.E. SHARP[1] & STEVEN K. MITTWEDE[1,2]

[1] Department of Earth and Ocean Sciences, University of South Carolina, Columbia, South Carolina 29208, USA (E-mail: sharp@sc.edu)
[2] Müteferrika Consulting and Translation Services Ltd., P.K. 290, Yenişehir, TR–06443 Ankara, Turkey

Received 01 April 2009; revised typescript received 18 February 2010; accepted 14 May 2010

Abstract: A mineralogical, mineral-geochemical and ^{14}C geochronological study of slags, previously identified as copper slags, in the Yapraklı area (Çankırı Province) of central Anatolia, has demonstrated that these are late-medieval iron slags consisting mainly of fayalite, glass, plagioclase, titanaugite, ulvöspinel and metallic iron. Because of the high lime content, relative to other medieval and Roman slags, these slags are quite anomalous in their lack of both modal and normative wüstite. Further study of these sites could shed light on the mining history and smelting methods of central Anatolia during a relatively obscure period of major socio-ethnic transition.

Key Words: iron slag, plagioclase, titanaugite, ulvöspinel, fayalite, leucite, iron smelting, late-medieval

Yapraklı (Çankırı, Türkiye) Yöresindeki Ortaçağa Ait Olan Plajiyoklaz ile Titanojiti İçeren Demir Cürufları

Özet: Yapraklı (Çankırı, İç Anadolu) civarında bulunan ve daha önce bakır cürufları düşünülmüş olan cüruflar üzerine mineralojik, mineral-jeokimyasal ve ^{14}C jeokronolojik çalışmaların sonuçlarıyla bu cürufların geç-ortaçağa ait demir cürufları olup fayalit, cam, plajiyoklaz, titanojit, ulvöspinel ve metalik demirden ibaret oldukları tespit edilmiştir. Diğer ortaçağa ve Romalılara ait olan cüruflara nazaran, yüksek CaO değerleri yüzünden bu cüruflarda wüstitin modal ve normatif olarak bulunmaması müstesnadır. Bu cüruf zuhurları üzerine daha fazla araştırmanın yapılmasıyla İç Anadolu'nun önemli ama az bilinen sosyo-etnik geçiş döneminin madencilik tarihi ve o dönemde uygulanmış olan izabe yöntemlerine ışık tutabilecek.

Anahtar Sözcükler: demir cürufu, plajiyoklaz, titanojit, ulvöspinel, fayalit, lösit, demir izabesi, geç-ortaçağ

Introduction

While investigating the geology of copper occurrences in central Anatolia and especially those in the vicinity of Ankara, it came to our attention that de Jesus (1978) had identified six groups of sites of extensive copper exploitation. One of these regional groups, Yapraklı (no. 2), lies 110 km NE of Ankara in the Çankırı Province, and trips were made to locate possible sources of copper in the area. As a guide to possible sites, additional detail was obtained from de Jesus' dissertation (1980) that focused on a series of 18 slag sites (de Jesus 1980, p. 240–246); a picture of one of these, Damlu Yurt Başı, can be found in de Jesus (1973, p. 72).

Upon examining a few of the listed sites, it quickly became evident that all of the sites included in the Yapraklı area were in fact iron slags which, when broken with a rock hammer, showed prills of iron rather than copper. The lack of any copper in these slags is also clear from the slag analyses provided by de Jesus (1980, p. 240–246). As found later, in the survey by Seeliger *et al.* (1985, p. 601), these slags were definitely identified as iron slags, and those authors thought that the slags were quite recent in age. While the immediate Yapraklı area does not have copper (other than insignificant showings near Urvay, Yapraklıdağ-Panayır, Tuhtköy, and Kiriş (Gerişköy); e.g., Coulant 1907; Maucher 1937; Ryan 1957; MTA 1972), copper ore is present elsewhere in the Çankırı Province, including in the mountains between Şabanözü and Eldivan (de Jesus 1980, p. 238–239; MTA 1972, p. 65) and at Hisarcıkkayı (de Jesus 1980, p. 240).

In so far as these iron slags consist of small isolated occurrences over a confined but fairly widespread area around Yapraklı, it seemed appropriate to take a closer look at the nature of these slags. However, it should be noted here that the source(s) of the iron ore remains uncertain. Hematitic iron formation (radiolarite?) was observed at one location near Damlu Yurt Başı (Table 1), and Upper Cretaceous radiolarites – some ophiolite-related (e.g., those in the vicinity of Eldivandağı; Figure 1) – have also been mapped in some detail – for example, those described in the Hisarköy Formation along strike to the SW near Çandır (Akyürek *et al.* 1988). There is only passing mention of iron ore in the geological literature pertaining to the Çankırı Province (e.g., Nowak 1927; Maucher 1937; Ryan 1957, p. 89; Budanur 1977, p. 115), and most of the iron prospects that have been mentioned are in Çerkeş County in the western part of the province (Figure 1) and, thus, are not germane to the present study.

Geological Setting

Although the town of Yapraklı itself is underlain by Oligocene–Lower Miocene evaporitic sediments and undifferentiated Pliocene clastic materials, the area to the N and NE – in which the studied slag occurrences are located – is underlain mainly by Mesozoic basic and ultrabasic ophiolitic rocks, Upper Cretaceous pillow lavas and associated sediments, along with patches of Upper Cretaceous clastic and carbonate rocks (Uğuz *et al.* 2002).

Location and Age

The studied slag sites (Figure 1 and Table 1) are spread over an area of about 100 km^2 in the Köroğlu Range north and east of Yapraklı at elevations typically above 1500 m. As illustrated by the site at Sünnük Bolukdağı Dömeke (99-04), all are found in upland meadows and forest quite far even from small streams (Figure 2a). As indicated by de Jesus (1980, p. 240; see also Seeliger *et al.* 1985, p. 601) and consistent with our own observations, the amount of slag ranges from several kg to a few thousand tonnes (Figure 2b). The individual pieces of slag are generally scoriaceous (Figure 2c) and are typically 8–10 cm in diameter. While some pieces were glassy with vesicles (Figure 3a, b) and some were dense and compact (Figure 3c), none showed any flow features such as layering or ropey surfaces. Moreover, none of the slag pieces showed any signs of green colouration or white coatings which might be derived from the oxidation of copper or lead, respectively. All of the slag heaps are notable for the lack of any materials other than slag (Figure 2b), not even pieces of ore – although Seeliger *et al.* (1985) reported the presence of hematitic ore at their site TG 160A – or even ceramic fragments, including those that could have come from tuyeres.

When the slag was broken open with a rock hammer, small pieces of charcoal were often observed (Figure 3d). Similarly, when broken open with a rock hammer, small pieces of iron were widely observed and, in some cases when sawed open with a rock saw, whole pieces of iron were occasionally found (Figure 2d). In so far as neither de Jesus (1980) nor Seeliger *et al.* (1985) reported a specific age for these slags, charcoal from selected slag fragments from a few of the sites were submitted for AMS radiocarbon dating. As will be discussed below, the age turned out to be late-medieval rather than the anticipated recent age suggested by Seeliger *et al.* (1985).

Slag Mineralogy

A number of the slag samples were sectioned with a diamond saw and, because the slags are generally opaque at standard thin-section thickness, thick polished sections were prepared. To capture a full range of variation in the slags, 13 sections were prepared from six sites. The sections were carbon-coated and then viewed as back-scattered electron (BSE) images on an electron microprobe (Cameca SX-50). Various phases in the slag specimens were selected for analysis using grey-scale contrast and also grain shape. Examples include: very bright round grains; small square bright grains; elongate platy dark grains; blocky dark-grey grains; anhedral medium-grey grains; elongate platy medium-grey grains; large rounded dark grains; large rounded light-grey grains and a light-grey matrix locally with very fine laths.

Quantitative analyses of the various slag phases were performed on an electron microprobe (Cameca SX-50) equipped with four wavelength dispersive

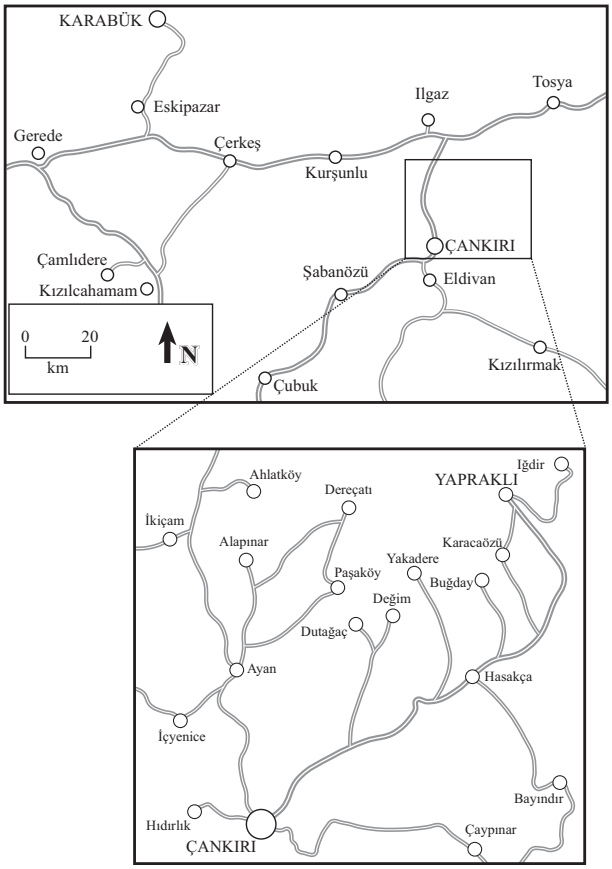

Figure 1. Location map of Yapraklı.

counters. The acceleration voltage was 15kV with a beam current of 10 nA, with a slightly defocused beam of 5 μm. Standards used were fayalite for Fe-Kα, synthetic MnO_2 for Mn-Kα, ilmenite for Ti-Kα, benitoite for Ba-Lα, chromite for Cr-Kα, diopside for Ca-Kα, microcline for K-Kα, apatite for P-Kα, olivine for Si-Kα, garnet for Al-Kα, olivine for Mg-Kα, and albite for Na-Kα. Dwell times were 30 seconds for major elements, 50 seconds for minor elements and 15 seconds for background. Observed intensities were adjusted for ZAF using the PAP correction program (Pouchou & Pichoir 1991) supplied with the microprobe.

The slags, in roughly 'hand-sized' pieces, either have the texture of a ceramic with abundant vesicles, or are vesicular glass. The ceramic-like slags consist of plagioclase with varying amounts of titanaugite and minor amounts of ulvöspinel, all in a matrix of glass or fayalite and glass. The distinct crystal outlines of the plagioclase and ulvöspinel suggest they were the first phases to appear and were followed by titanaugite and, subsequently, fayalite with glass or simply glass. Detailed descriptions of the recognized phases are given below.

Iron

Metallic iron occurs in four different forms within the slag: as large round grains (Figure 4a), in some cases with distinct cracks (Figure 4b); as beads and ovoid masses (Figure 4c); and as skeletal crystals (Figure 4d) or as ovoid skeletal patches consisting of numerous globulites, with as much as 50% included glass (Figure 7b). The cracks observed (Figure 4b) in one of the round prills are suggestive of precipitated

Table 1. Iron slag locations of the Yapraklı area.

Site	Site Name	Latitude	Longitude
99–01	Kumlu Çukur Mevkii (Yakadere Köyü)	N40 43′ 26″	E33 43′ 58″
97–06	Panayır Tepesi	N40 47′ 28″	E33 46′ 58″
99–02	Çayırlıdere (Akyolun tepesi)	N40 47′ 28″	E33 45′ 15″
97–07	Dipyurt	N40 48′ 47″	E33 44′ 01″
99–03	Dedeköy	N40 48′ 32″	E33 43′ 54″
99–04	Sünnük Bolukdağı Dömeke (Deresi üstü)	N40 49′ 51″	E33 45′ 15″
99–05	Kapaklık Mevkii (Yukarıöz)	N40 49′ 49″	E33 48′ 09″
99–06	Damlu Yurt Başı	N40 50′ 22″	E33 48′ 11″
	nearby BIF(radiolarite?)	N40 50′ 34″	E33 48′ 17″
99–07	Karatepe	N40 50′ 47″	E33 48′ 40″
	(Karatepe'deki "demir boku" mevkii) nearby Tekmen tarlası	N40 50′ 42″	E33 48′ 34″
99–08	Mustafa Ünür tarlası	N40 50′ 30″	E33 49′ 50″
99–09	Gökçukur Deresi	N40 50′ 39″	E33 49′ 22″
99–10	Asarcık Yaylası (Çapanın köprüsü)	N40 50′ 45″	E33 49′ 34″
99–11	Kaşyaylası (lower)	N40 50′ 21″	E33 50′ 11″
99–12	Kaşyaylası (upper)	N40 50′ 21″	E33 49′ 56″

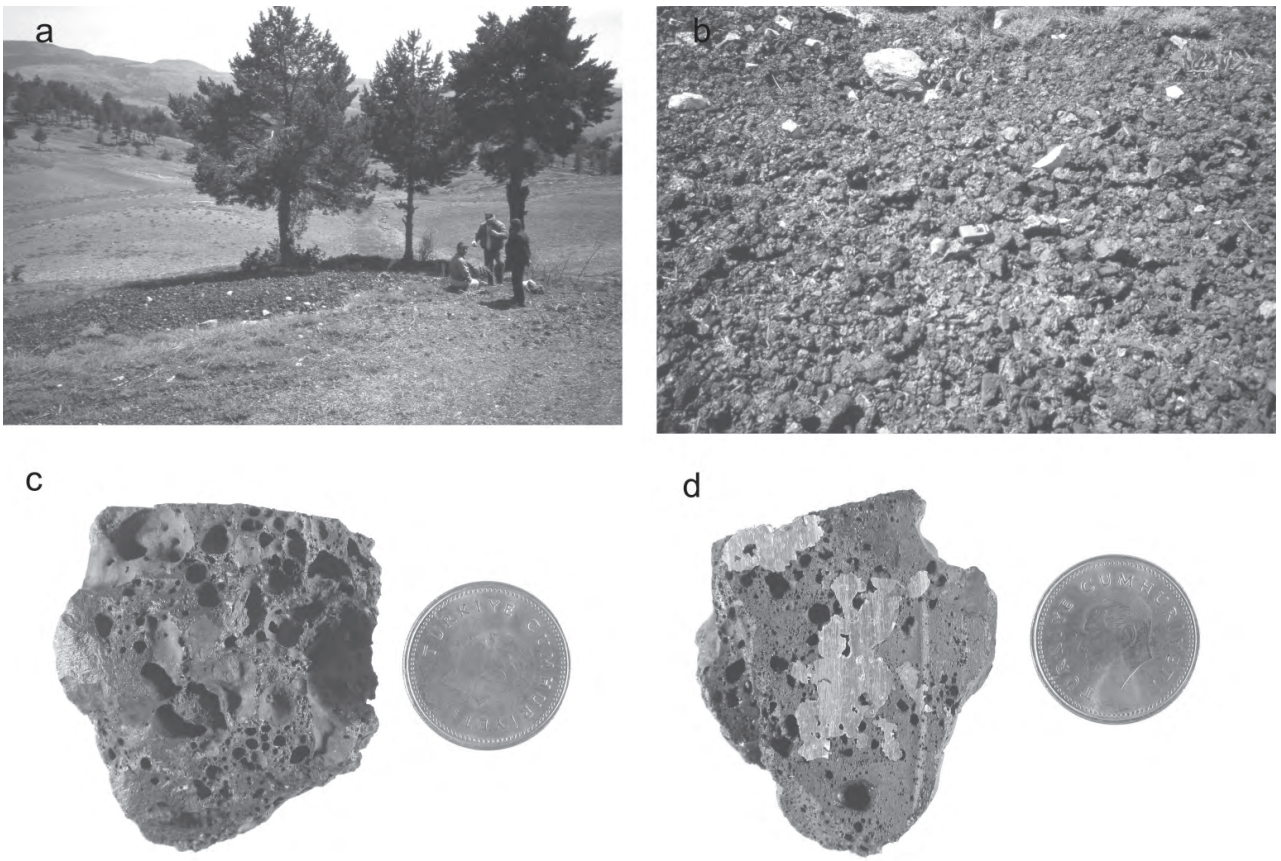

Figure 2. Slag site of Sünnük Bolukdağı Dömeke (99-04). **(a)** View of site relative to the upland meadows, with SKM and two local guides. **(b)** Typical view of slag exposure. **(c)** Typical example of scoriaceous slag. **(d)** Sawed piece of scoriaceous slag showing embedded piece of metallic iron. Coin diameter is 2.50 cm.

graphite. However, checking the crack with the electron beam showed only the presence of epoxy; if there had been graphite where the crack appears, it was lost or removed during the preparation of the probe section. Tests were also made to see if there was detectable carbon in any of the iron. This was done using the microprobe by spectrometer scans with crystal PC1. No carbon, beyond that expected from the carbon coating, was observed. Compositions measured with the microprobe averaged 99.46% iron (Table 2) when calibrated using a fayalite standard. A few grains (Table B1: 14, 50, 53, 55) have elevated Si contents of 1.29%, and a few grains (Table B1: 75, 76) have elevated P contents of 1.27%.

Plagioclase

Plagioclase occurs as elongate platy dark grains and is consistently observed as distinct crystals, suggesting that it is one of the earliest phases to crystallize in the slag. It occurs as elongate laths in glass (Figure 5a), as elongate laths in devitrified glass (Figure 5b), with equigranular subophitic texture comprising distinct laths in a matrix of titanaugite and fayalite (Figure 5c), as equigranular grains in a matrix of titanaugite and fayalite (Figure 5d), and as micro-ophitic zones with titanaugite and laths of fayalite (Figure 6a).

Leucite

Leucite is present in a limited part of one section as equigranular grains embedded in a matrix of titanaugite and fayalite (Figure 6b), and is discussed here because of its textural resemblance to some of the plagioclase. In Figure 5d, leucite grains are embedded in a similar matrix but are medium grey instead of the dark grey of the plagioclase.

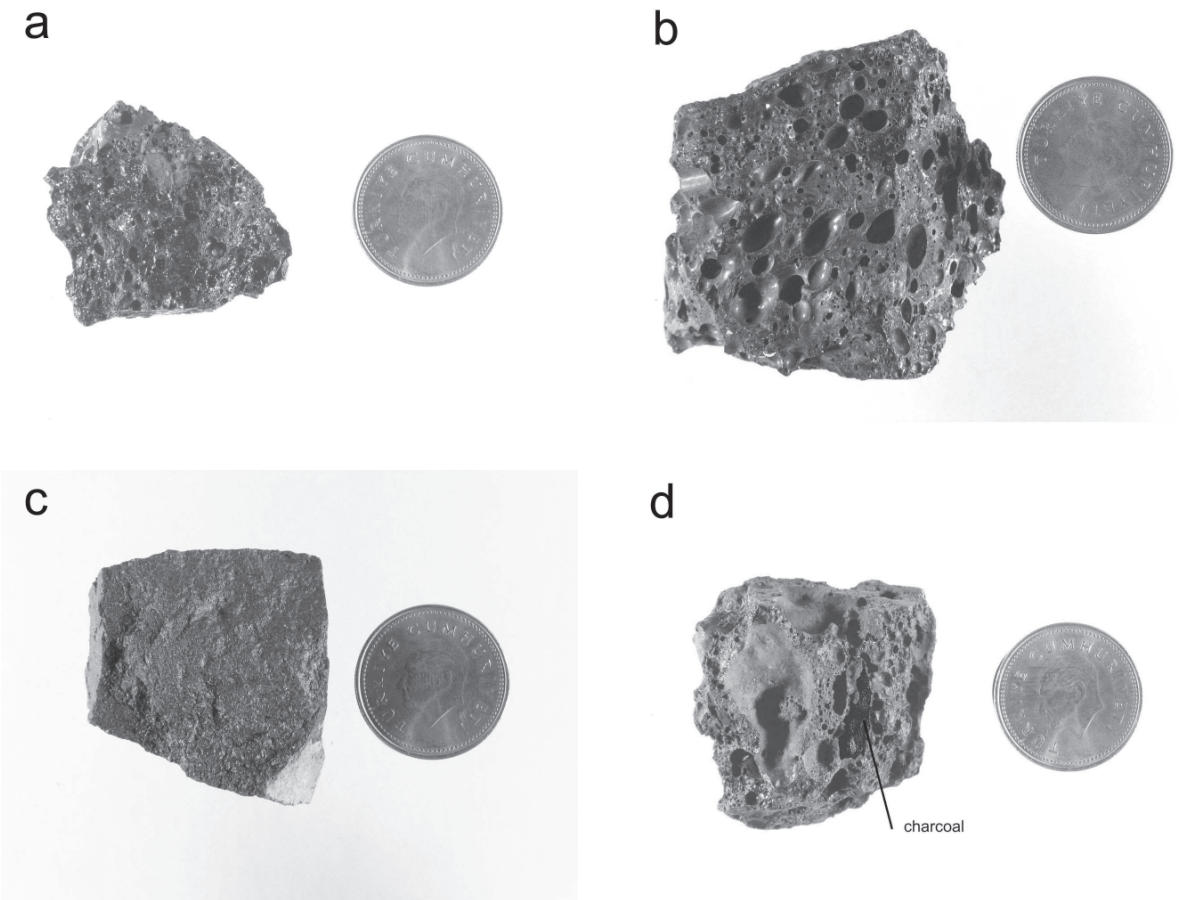

Figure 3. Other examples of slag pieces. **(a)** Vesicular glassy slag from Dipyurt (97-07). **(b)** Glassy slag with large vesicles from Damlu Yurt Başı (99-06). **(c)** Dense compact slag from Kumlu Çukur Mevkii (99-01). **(d)** Charcoal embedded in scoriaceous slag from Sünnük Bolukdağı Dömeke (99-04). Coin diameter is 2.50 cm.

Titanaugite

Titanaugite occurs with a subophitic texture as anhedral, medium-grey grains between laths of plagioclase and bounded by fayalite (Figure 5c), as anhedral grains between large grains of plagioclase, as anhedral grains among large grains of leucite (Figure 6d), and as micro-ophitic slag (Figure 6a).

Ulvöspinel

Ulvöspinel appears in most of the probe sections as small bright grains with blocky outlines (Figures 4c, 5a, b & 6c), and as very small crystalline grains embedded in glass between crystals of fayalite (Figure 6d). It is thought to be an early phase because it is euhedral in almost all cases. Because of its small grain size, it was quite difficult to find ulvöspinel grains large enough to analyse. When analysed, the observed ulvöspinel is lower in titanium than the ideal, but this has been taken up by chromium (Table 2); thus it might properly be termed a Cr-ulvöspinel. Further, the totals tend to be on the low side. Because the analyses of chromites have reasonable totals, it is suspected that the low totals are the result of the ulvöspinel capturing any ferric iron present in the slag.

Fayalite

Fayalite occurs as feathery elongate laths typically embedded in glass (Figures 4c & 6c, d), and as marginal grains adjacent to plagioclase (Figures 3a & 5c) or leucite (Figure 6b). Fayalite, along with glass, is the dominant phase in the groundmass of the slag.

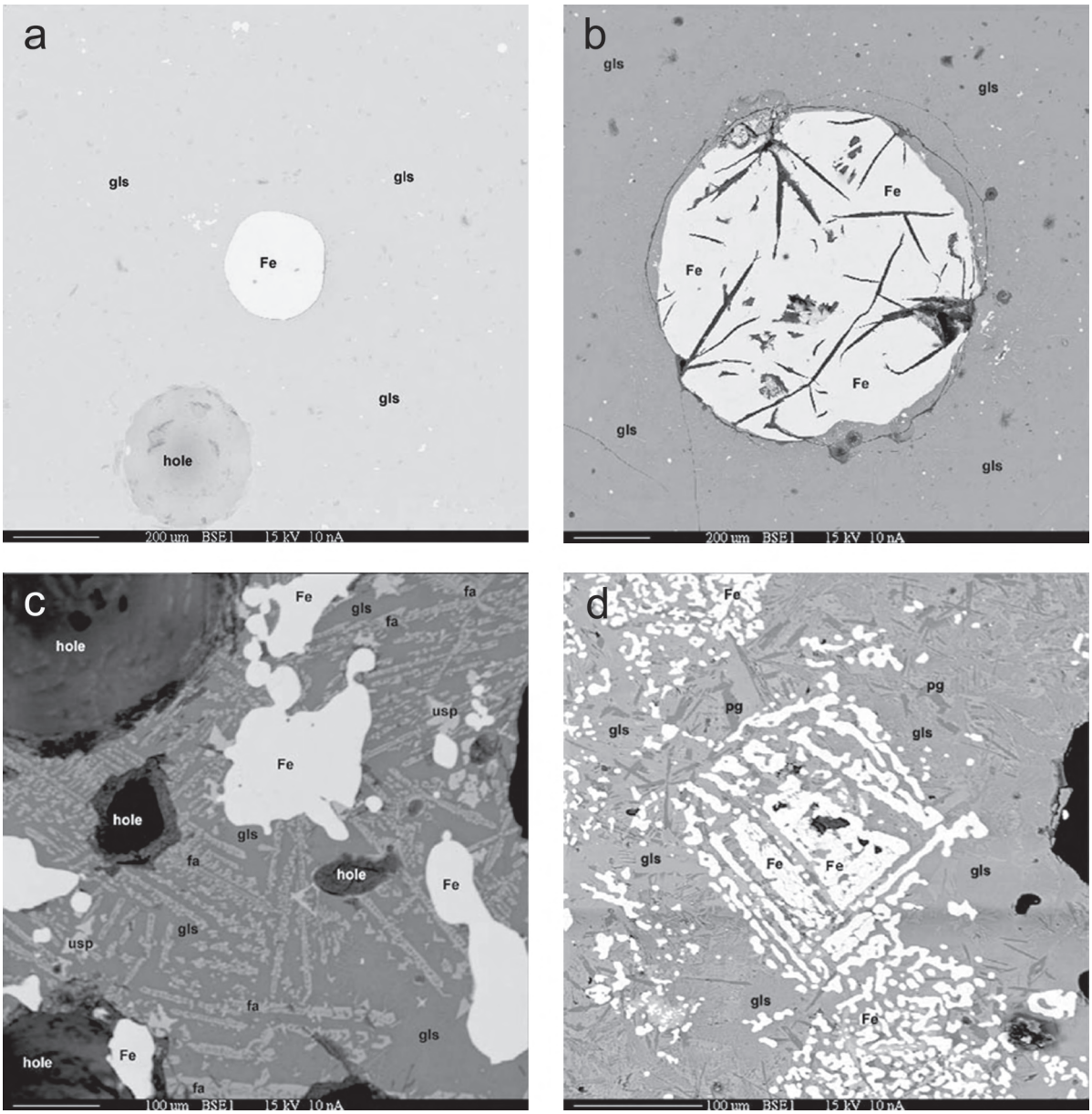

Figure 4. **(a)** A backscatter image from scene 2 of probe section 99-10B showing a prill of metallic iron (Fe) embedded in glass (gls). **(b)** A backscatter image from scene 2 of probe section 99-06C showing an iron prill (Fe) with prominent cracks embedded in glass matrix (gls). **(c)** A backscatter image from scene 4 of probe section 99-04C showing ovoid iron prills and beads (Fe) in a matrix of fayalite laths (fa) and glass (gls), with scattered grains of ulvöspinel (usp). **(d)** A backscatter image from scene 7 of probe section 99-03A showing a skeletal crystal of iron (Fe) along with skeletal patches of iron composed of numerous globulites; these are embedded in a matrix of glass (gls) with laths of plagioclase (pg).

Table 2. Composition of the iron phase.

Average (no.)	wt.	Si	Ti	Al	Fe	Mn	Mg	Ca	Na	K	P	Ba	Cr	Total	Source
Iron (31)	%	0.20	0.11	0.02	99.46	0.08	0.02	0.06	0.02	0.04	0.22	0.13	0.25	100.60	B1

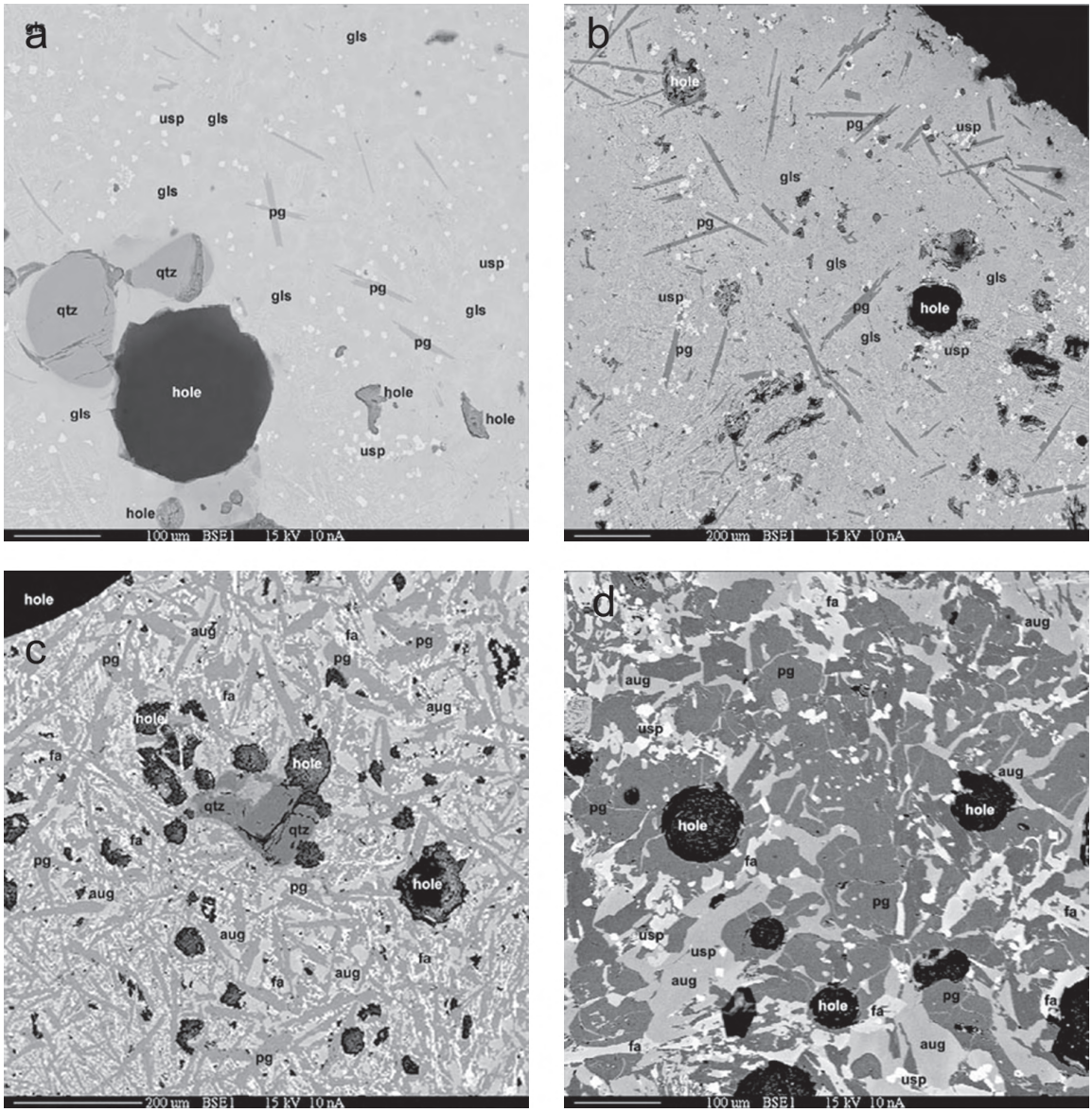

Figure 5. **(a)** A backscatter image from scene 5 of probe section 99-08A showing laths of plagioclase (pg) in a matrix of glass (gls). Also in the scene are small blocky crystals of ulvöspinel (usp), residual grains of quartz (qtz) and holes. **(b)** A backscatter image from scene 2 of probe section 99-10A showing numerous laths of plagioclase (pg) in a devitrified matrix of glass (gls) with scattered small crystals of ulvöspinel (usp). **(c)** A backscatter image from scene 1 of probe section 99-06B showing plagioclase (pg) as part of a subophitic texture with titanaugite (aug) and fayalite (fa). Note the presence of a residual quartz grain at the centre of the scene. **(d)** A backscatter image from scene 4 of probe section 99-06B showing anhedral grains of plagioclase (pg) as part of an ophitic texture with titanaugite (aug) and fayalite (fa).

Hematite

Hematite in the few images in which it was observed is present as anhedral or ovoid grains (Figure 7a). At the centre of Figure 6d, metallic iron (Fe) surrounds a small hole which in turn is surrounded by a grain of hematite (hm). In the BSE images, the hematite is similar in brightness to fayalite but the grains are much larger and more irregular. Analyses of the hematite (Table 3) average 90%, notably less than the 93% expected for magnetite or the 100% expected for wüstite.

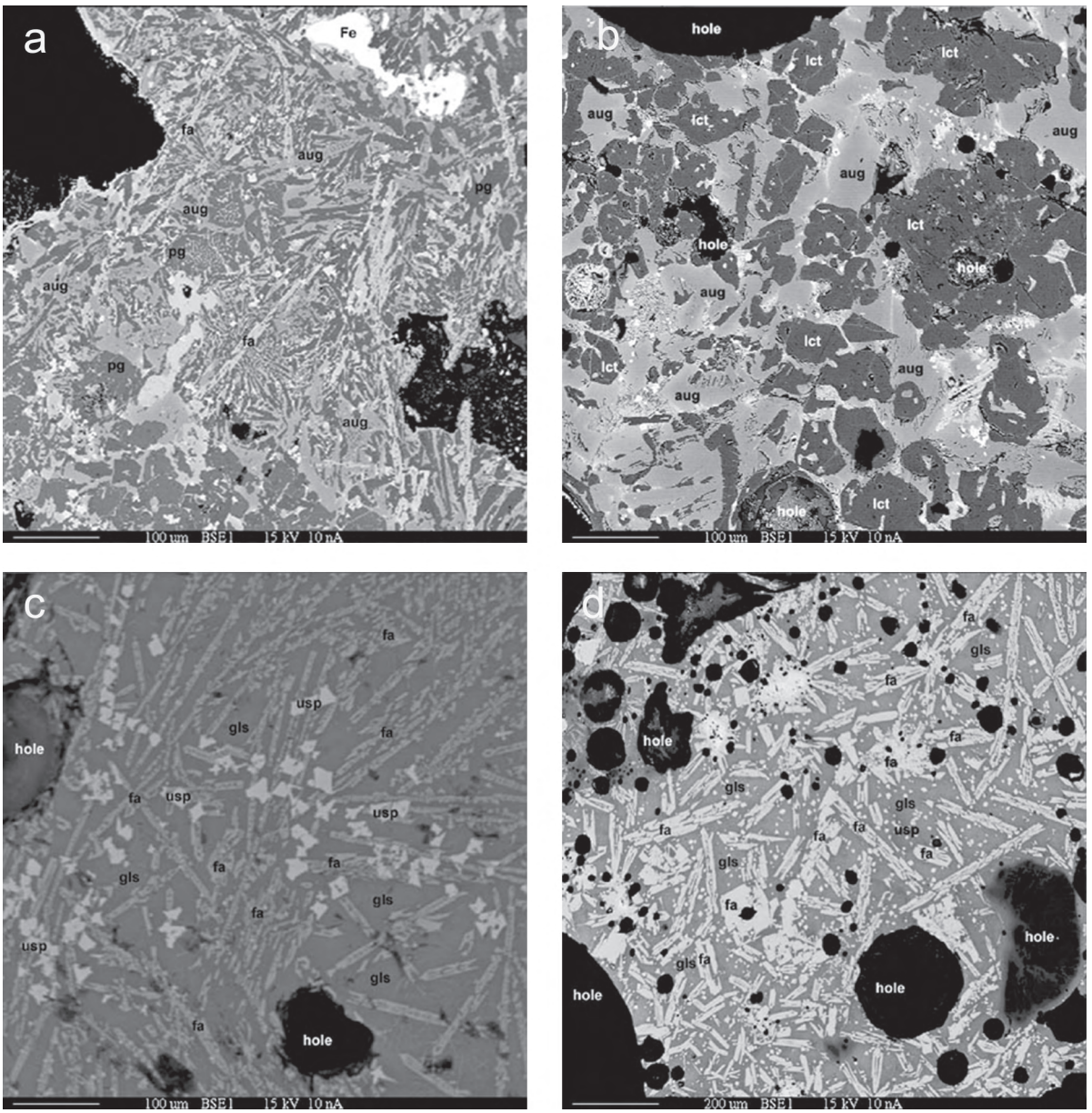

Figure 6. **(a)** A backscatter image from scene 4 of probe section 99-06B showing laths of plagioclase (pg) as micro-ophitic zones with titanaugite (aug) and laths of fayalite (fa). **(b)** A backscatter image from scene 5 of probe section 97-07A showing anhedral grains of leucite (lc) embedded in a matrix of titanaugite (aug) and fayalite (fa). Note the resemblance of the leucite here to the plagioclase in Figure 5d. **(c)** A backscatter image from scene 3 of probe section 99-04C showing fayalite (fa) embedded in a matrix of glass (gls). Note the much brighter and scattered blocky crystals of ulvöspinel (usp). **(d)** A backscatter image from scene 4 of probe section 99-08A showing laths and blocky crystals of fayalite (fa) embedded in a matrix of glass (gls). Ulvöspinel (usp) is present as bright, very fine-grained, blocky crystals in the glass.

Chromite

Chromite occurs as round grains in almost every section examined (e.g., Figure 7b). The consistent appearance of chromite, its rounded shape, and its resistance to dissolution in the slag suggest that the observed grains are residual grains mixed either in the hematitic ore or as part of silica sands that were presumably added as fluxes.

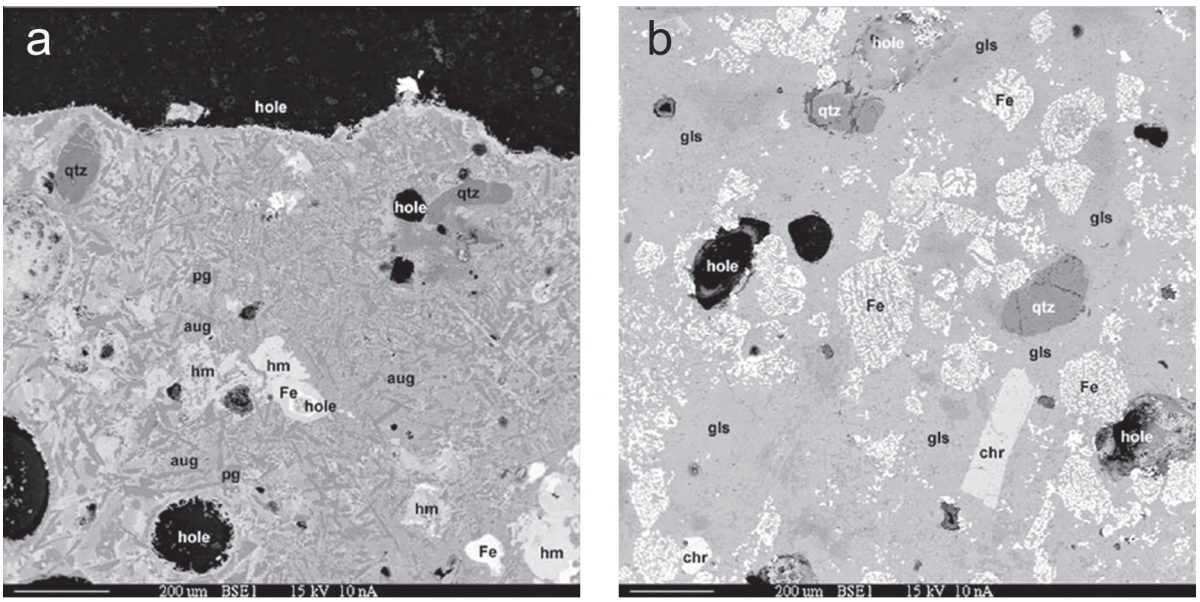

Figure 7. **(a)** A backscatter image from scene 2 of probe section 97-07A showing anhedral and ovoid grains of hematite (hm) embedded in a matrix of plagioclase (pg) and titanaugite (aug). Note the presence of metallic iron (Fe) and residual grains of quartz (qtz). **(b)** A backscatter image from scene 6 of probe section 99-03A showing residual grains of chromite (chr) and quartz (qtz) along with ovoid skeletal patches of metallic iron (Fe). These are all embedded in glass (gls) which, on a microscale, has exsolved fayalite (not visible).

Table 3. Compositions of mineral phases.

Average	(no.)	wt	SiO_2	TiO_2	Al_2O_3	FeO	MnO	MgO	CaO	Na_2O	K_2O	P_2O_5	BaO	Cr_2O_3	Total	Source
Plag.	(22)	%	49.78	0.19	28.82	1.49	0.02	0.33	14.39	2.11	1.17	0.03	0.05	0.02	98.39	B2
An70		%	50.54	.0	31.70	.0	.0	.0	14.36	3.40	.0	.0	.0	.0	100.00	
Leucite	(4)	%	55.01	0.09	21.94	0.03	0.00	0.00	0.00	0.64	19.12	0.01	0.00	0.00	96.84	B3
Ideal		%	55.06	.0	23.36	.0	.0	.0	.0	.0	21.58	.0	.0	.0	100.00	
Ti-augite	(16)	%	43.54	3.59	8.41	15.77	0.31	6.80	18.52	0.30	0.55	0.26	0.07	0.16	98.28	B4
Natural		%	47.11	3.75	3.00	15.56	.0	16.85	13.54	0.22	0.02	.0	.0	.0	99.96	
Natural		%	40.28	3.85	10.30	12.73	.0	7.78	23.57	0.36	.0	.0	.0	.0	99.06	
Ulvöspinel(9)		%	0.20	25.89	4.83	58.57	0.48	1.22	0.25	0.02	0.08	0.04	0.19	3.93	95.68	B5
Ideal		%	0.00	35.73	0.00	64.27	0.00	0.00	0.00	0.00	0.00	0.00	0.00	0.00	100.00	
Natural		%	0.33	26.76	2.31	64.29	0.61	1.93	0.59	.0	.0	.0	.0	0.38	97.48	
Fayalite	(6)	%	32.34	0.24	0.15	51.12	0.75	14.62	0.84	0.02	0.07	0.07	0.08	0.06	100.37	B6
Fa66		%	32.95	.0	.0	52.01	.0	15.03	.0	.0	.0	.0	.0	.0	99.99	
Fayalite	(7)	%	30.51	0.36	0.58	61.44	0.90	4.59	0.98	0.06	0.13	0.23	0.07	0.04	99.91	
Fa88		%	30.62	.0	.0	64.44	.0	4.93	.0	.0	.0	.0	.0	.0	99.99	
Hematite	(7)	%	0.24	0.43	0.10	88.52	0.12	0.04	0.10	0.04	0.05	0.14	0.12	0.14	90.03	B7
Ideal		%	.0	.0	.0	89.98	.0	.0	.0	.0	.0	.0	.0	.0	89.98	
Chromite(28)		%	0.04	0.18	19.01	49.36	20.49	0.19	10.38	0.04	0.02	0.02	0.02	0.08	99.84	B8
Natural		%	.0	0.69	13.36	52.77	21.78	0.20	10.31	0.28	.0	.0	.0	.0	99.39	
Quartz	(32)	%	98.20	0.02	0.35	0.28	0.01	0.03	0.10	0.04	0.17	0.03	0.03	0.01	99.27	B9
Ideal		%	100.00	.0	.0	.0	.0	.0	.0	.0	.0	.0	.0	.0	100.00	

Zircon

Zircon was observed as a single isolated grain. When observed in the BSE image, it is rounded like the chromite but is brighter and fluoresces when in the electron beam. It is probably a residual grain which accompanied any silica added as a flux.

Quartz

Quartz, like the chromite, was observed as residual undigested grains in a number of sections (Figures 5a, c & 7a, b). Consequently, the slags are relatively silica-rich. As checked by X-ray diffractometry, none of the residual quartz grains has been converted to either cristobalite or to tridymite. The x-ray diffraction work was carried out on a computer-controlled diffractometer (Scintag), and samples were scanned over a range of 4 to 65 degrees 2-theta using copper radiation. Quartz was easily detected but there was no indication of any lines for tridymite or cristobalite.

Glass

Glass ranges from composing almost the entire bulk of an individual piece of slag (Figures 1b & 4a) down to very small amounts of residual interstitial glass (Figure 6c) occurring as a matrix among the much larger complex of mineral grains. Overall, the glass is rich in both silica and lime (Table 4), and may be distinguished compositionally from all other phases by the presence of at least one percent potash; the potash content can range up to a maximum of seven percent (Table B13). Magnesia and titania are also important components of the glass. A careful examination of the glass compositions shows that they can be divided into six groups on the basis of their compositions. Overall the glasses are normative in anorthite-fayalite-wollastonite – quartz, and these glasses (Table 4) can be subdivided into high iron, low iron, high lime and high potash. It should be noted that, while the slags are high in lime and silica, wollastonite is scarce as an actual phase and neither tridymite nor cristobalite was observed as a separate phase. Some of the glasses are quite rich in K_2O and may be considered leucite-normative (Table B13). However, some of the glasses were not wollastonite-normative; these low-lime glasses had extra alumina which made them hercynite-normative, and a few were even mullite-normative.

Discussion

Age

The iron slags are well exposed with few signs of burial which *could* suggest that the slags are relatively recent in age (Seeliger *et al.* 1985, p. 601). However, charcoal embedded in slag fragments (Figure 3d) from four of the slag sites was submitted for AMS radiocarbon dating, and the results of these analyses revealed that they are late-medieval in age. Ages ranged from 486 yrs BP to 571 yrs BP, with an average age of 533 yrs BP and a standard error of 24 yrs BP (Table 5). A graph of C-14 age (Stuiver & Reimer 1993; Reimer *et al.* 2004) versus calibrated calendar age (Figure A1) gives an expected primary calendar age of 1412 AD and a secondary calendar age of 1336 AD.

Considering the number of slag heaps and their rather narrow age range, this would suggest some event, such as a military campaign, might have precipitated a sudden push for the local production of iron.

If one accepts the primary age of 1412 AD, this roughly corresponds to the time when the Ottoman sultan, Mehmed, led an expedition to Anatolia in 1417 against the emir of Sinop, which ultimately placed Mehmed in control of Kastamonu and its copper mines (Imber 2002, p. 21). Kastamonu lies just 80 km directly north of Yapraklı.

Table 4. Composition of glasses.

Average		wt	SiO_2	TiO_2	Al_2O_3	FeO	MnO	MgO	CaO	Na_2O	K_2O	P_2O_5	BaO	Cr_2O_3	Total	Source
High–iron	(42)	%	46.45	3.34	11.83	20.88	0.39	2.01	10.60	0.78	2.23	0.26	0.08	0.07	98.90	B10
Low–iron	(25)	%	51.52	4.70	14.55	8.41	0.54	3.18	11.55	0.95	2.63	0.11	0.13	0.25	98.51	B11
High–lime	(16)	%	51.01	4.72	12.94	7.31	0.62	2.68	15.92	0.88	2.16	0.16	0.09	0.21	98.69	B12
Potash	(8)	%	58.46	4.90	12.91	6.01	0.37	0.88	6.33	1.13	5.98	0.28	0.09	0.07	97.39	B13
Low–lime	(6)	%	49.30	2.97	13.26	24.96	0.61	0.64	4.17	0.74	1.73	0.35	0.04	0.02	98.79	B14
Alumina	(4)	%	59.54	0.46	23.40	2.15	0.03	0.63	4.70	2.06	5.07	0.06	0.02	0.04	98.14	B15

Table 5. ^{14}C ages of selected Yapraklı slags.

Site	Sample	$D^{13}C$(mils)	Fraction Modern	^{14}C	age BP	ca Cal age
97–07	GX23363	–24.7	0.9387±0.0060	510±60	AD	1334/1420±27
99–04	AA65875	–26.8	0.9413±0.0062	486±53	AD	1427/– ±28
99–05	AA65876	–22.6	0.9319±0.0046	567±40	AD	1336/1402±13
99–10	AA65878	–23.9	0.9314±0.0052	571±45	AD	1335/1401±13
–	Average	–24.5	–	533±24	AD	1414±14

If one accepts the secondary age of 1336 AD, then this corresponds to an obscure time in history when the Turks immigrated into Anatolia and the region was divided into a series of local principalities between the end of the Seljuk realms and the rise of the Ottomans (Imber 2002, p. 7–9). However, if the age represents the average age of the wood, then the production of iron could correspond to a somewhat later period, such as around 1461 when Mehmed sent a fleet along the Black Sea coast (as well as an army overland) to capture Sinop and Trabzon (Imber 2002, p. 31).

Composition

The slags of the Yapraklı area are all relatively similar in composition and texture. While they range from nearly complete glass through to scoriaceous ceramic, they are in the form of lumps with no indication of smooth ropey surfaces or interior banding that would suggest the presence of any liquid flow. Although originally described as copper slags by de Jesus, they are definitely iron slags. Compositionally the slags are high in silica and lime along with alumina, moderate in titania and are low in manganese. Where found embedded in the slag, metallic iron takes the form of lumps, rounded prills or skeletal patches. The rounded prills would appear to be simply solidified liquid iron. One of these prills had an observed silicon content of 1.29% (Table B1). Such silicon contents are known to occur in cast irons from the reduction of silica to Si under strongly reducing conditions (Partington 1939, p. 960). The observed P in one prill is suggestive that the iron phase may have absorbed some reduced P; it is suspected this is probably analytical error in so far as there is no indication of any P-bearing phases (such as apatite), nor is there notable P in any of the glass in the slag. Any dissolved carbon that might be in the iron was not detectable with the microprobe.

Pure iron melts at a temperature of 1534 °C (Hansen 1958, p. 354), well beyond the temperatures expected with these slags. However, the presence of carbon can reduce the solidus to 1153 °C and, while that places the molten iron in the range of the slag, there is no indication of detectable dissolved carbon, exsolved graphite or iron carbide leaving unresolved how these oblate grains – which resemble droplets of liquid – could be found within the expected temperature range of these slags. However, the skeletal patches of iron do appear to be the result of solid-state reduction, and this places them well within the formation temperatures of the slag.

Distinct crystal outlines, along with individual grains completely surrounded by glass, suggest that plagioclase and ulvöspinel were the first phases to crystallize from the molten slag. The presence of crystalline plagioclase together with the composition of the glasses (discussed below) suggest that the slag compositions will fall near the ternary phase diagram $CaAl_2Si_2O_8$-SiO_2-FeO in the four component phase diagram of CaO-FeO-Al_2O_3-SiO_2. The ulvöspinel grains are quite small and thus it was difficult to obtain microprobe analyses, which are unaffected by the size of the electron beam; this accounts in part for the low totals observed. If one eliminates likely contaminants (such as silica and barium) from the surrounding glass, an average resulting analysis is given in Table 6. If one normalises this analysis and partitions the various ions over the tetrahedral and octahedral positions, and accepts the classic substitution of 2 Fe^{3+} = Fe^{2+} + Ti^{4+} (Bosi *et al.* 2008, p.

Table 6. Composition of ulvöspinel in the Yapraklı slags.

Average observed		Normalised number of ions with 4O			Corrected observed	
TiO_2	25.89	Mg	0.0687		TiO_2	25.90
Al_2O_3	4.83	Mn	0.0154	1.0	Al_2O_3	4.83
FeO(T)	58.57	Fe^{2+}	0.9159		FeO	52.31
MnO	0.48				Fe_2O_3	6.96
MgO	1.22	Fe^{2+}	0.7352		MnO	0.48
Cr_2O_3	3.93	Fe^{3+}	0.1976	1.0	MgO	1.22
		Al	0.0672		Cr_2O_3	3.92
Total	94.92					
		Ti	0.7352		Total	95.62
		Al	0.1476	1.0		
		Cr	0.1172			

1315), then the ion distributions should be as shown in the middle column of Table 6. This distribution of ions suggests that the average observed ulvöspinel has an Fe^{3+} of 0.198 and an Fe^{2+} of 1.651 and an Fe^{3+} / Σ Fe = 0.11. The latter ratio (as well as the TiO_2/FeO_T ratio) falls in the mid-range of synthetic ulvöspinels grown under oxygen-fugacity conditions of 10^{-11} to 10^{-17} (Bosi *et al.* 2008, p. 1315). The ion stoichiometry would suggest an average analysis for the ulvöspinel as given in the last column of Table 6.

In a part of at least one section, leucite is a prominent phase consisting of anhedral grains embedded in titanaugite and fayalite. To have leucite as a separate phase requires the presence of significant amounts of potash. While the source of silica in the slag could be sand with muscovite or potash feldspar, no evidence of any residual grains of potash feldspar was observed in any of the sections. A more likely source of potash would be the charcoal used in the smelting process.

Anhedral titanaugite appears as a distinct phase surrounding either leucite or plagioclase. With respect to the system $CaO\text{-}FeO\text{-}Al_2O_3\text{-}SiO_2$, the presence of this phase would correspond to hedenbergite. However, hedenbergite is not usually observed in that system if any liquid is present (Schairer 1942, p. 265), but only as a subsolidus phase. While in some titanaugite-bearing sections no glass was seen, it is uncertain that this observation can be extended to other sections. Furthermore, the presence of magnesia and titania may have stabilised this particular phase.

In one section anhedral grains, from which the results of microprobe analyses correspond to hematite, were observed. As described above, a progression from a hole to metallic iron to hematite was observed; this is the only image that suggests the presence of an ore grain. If this is correct, then the ore was either hematite or dehydrated goethite. If the ore was goethite, the low manganese in all phases including fayalite would suggest it could not have been a bog-iron, such as might be found in upland mountain meadows.

Fayalite, as described above, occurs as grains adjacent to leucite or plagioclase, and also occurs as feathery grains with glass in the groundmass of the slag. At very high magnifications, fayalite is readily observed as crystals with included glass. From this it is interpreted that the fayalite may be an exsolved phase from the quenched glass. Two different compositions of fayalite were found: Fa_{66} and Fa_{88}.

Four minerals are thought to be residual, resistate grains; these include hematite, quartz, zircon and chromite. One section containing a few grains of hematite was described above. A single grain of zircon was noted, and this was discovered by its fluorescence in the electron beam of the microprobe. In contrast to these scarce grains, quartz and chromite occur in several of the sections. The quartz is thought to be residual grains from any sand or sandstone that may have been used in the slagging process. They are rounded and show no evidence of conversion to either tridymite or cristobalite. This was confirmed by x-ray diffraction of silica-rich sections, in which no peaks of

either mineral were observed. The observed chromite grains were rounded and showed no signs of digestion by the slag. Chromite grains were relatively easy to find and were relatively abundant. It is thought that these grains, too, were part of any sand or sandstone that was used in the slagging process. Much of the area immediately north of Yapraklı is underlain by ophiolitic rocks, and chromite derived from these rocks would logically have been part of the sands of this area. We even wonder if these early miners might have tried to obtain iron from chromite.

Glass is ubiquitous, but ranges from making up nearly all to virtually none of a particular slag fragment. Microprobe analyses of the glasses show that 90% of the glasses were normative in anorthite-fayalite-quartz and wollastonite; that is, most of the iron slags analysed were high in silica and lime, moderate in titania and low in manganese. Unlike other medieval or Roman slags which have been described, none of the studied slag samples are normative in wüstite. Normative compositions were computed using observed minerals in the slag along with those expected within the observed portion of the CaO-FeO-Al_2O_3-SiO_2 phase diagram; that is, anorthite, fayalite, quartz and wollastonite. Additional phases, including hercynite, mullite and leucite, were calculated for those glasses for which they were required. For a majority of the slags, the compositions lie near the plane of the ternary phase diagram of $CaAl_2Si_2O_8$-SiO_2-FeO in the four component tetrahedron of CaO-FeO-Al_2O_3-SiO_2. For a smaller subset, the compositions would lie more toward the CaO apex. If one takes and renormalises the average high-iron glass composition (Table 4) to obtain An= 38.27, FeO= 23.28 and SiO_2= 38.45, this composition falls adjacent to the anorthite-tridymite cotectic at about 1200 °C. Similarly, if the average low-iron glass composition (Table 4) is renormalised to An= 48.13, FeO= 10.21, and SiO_2= 41.67, this composition also falls adjacent to the anorthite-tridymite cotectic at around 1300 °C (Figure 8). However, this calculation neglects any effect of normative wollastonite, which could lower the melting temperature by as much as 100 °C. Interestingly, no evidence of residual mineral grains was detected that might account for any of the titania, alumina, magnesia or lime. Because of the high lime content, it is suspected that limestone in some form was added along with sand or sandstone to form the smelting flux.

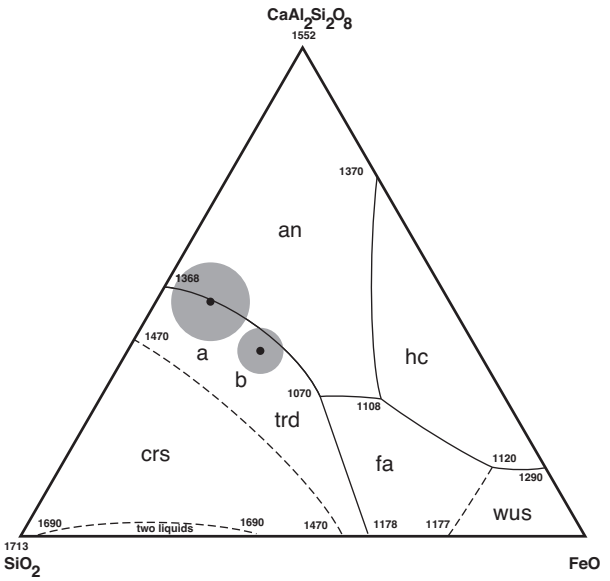

Figure 8. Ternary equilibrium diagram of the system $CaAl_2Si_2O_8$-FeO-SiO_2 (Schairer 1942) showing the phase relations among anorthite (an), tridymite (trd), cristobalite (crs), fayalite (fa), wüstite (wus), and hercynite (hc). For our samples: a– low-iron glasses; b– high-iron glasses. The black dots represent the centres of the respective sample groups, and the grey circles represent one standard deviation from each of those centres.

From the view of iron smelting at other medieval or Roman sites, these slags are anomalous in being wüstite-free. The mineralogy and the composition of the glasses indicate the slags were along the tridymite-anorthite cotectic. If one reviews the reports on slags from Roman and medieval Britain (Morton & Wingrove 1969, 1972), those slags carry wüstite-fayalite or wüstite-fayalite-hercynite with FeO contents of 50–80% instead of the average 8% and 20% observed here. In a review of optimum iron-slagging conditions (Rehren *et al.* 2007), two optima were found: one with fayalite-hercynite-tridymite at 1058 °C, and a second with wüstite-hercynite-fayalite at 1148 °C. In contrast, modern blast-furnace slags with melting temperatures of around 1350 °C are both modal and normative in melilite but carry less than 2% FeO (Josephson *et al.* 1949, p. 55, 65; Lee 1974, p. 26).

The nature of the smelting conditions at these sites should warrant further study. The slag heaps have no sign of any ceramic – not even that which might have

been derived from tuyeres. Unlike other slags of this age, they are wüstite-free because of the very high lime content. All of the sites are in upland meadows or forest far from any streams, all of which suggest that the furnaces probably used a natural draft. The true nature of the ore is also unclear. Certainly, there were no obvious signs of ore found with or around any of the slag heaps. Although hematite was reported at one site (TG 160A) by Seeliger *et al.* (1985), and grains of hematite were observed in one probe section, and some banded iron formation with hematite was observed near site 99-06, it is not at all certain that hematite was indeed the ore. It is commonly thought (Wertime 1980) that black sands were a likely ore in this region. Such black sands would be expected to have significant ilmenite or rutile. While the slags have moderate titania, no signs of any residual grains of magnetite, ilmenite or rutile were found in any of the slag sections. The flux for slagging was certainly local sandstone or river sands rich in quartz as evidenced by residual quartz and chromite grains as well as a single grain of zircon. The sand or sandstone must have been mixed with limestone. Both the sands and limestone are adequate to account for most of the other minor oxides found in the slag, including magnesia, alumina and titania. The presence of potash and soda in the slag is probably from ash resulting from the combustion of any charcoal fuel used in the smelting.

Conclusions

The slags from Yapraklı were found to be iron slags rather than copper slags as originally reported by de Jesus. The absence of any sediment covering the slags *might* have suggested they are relatively recent slags, but ^{14}C age dating of charcoal embedded in the slags suggests they are late-medieval. The iron slags are enriched in lime and silica such that plagioclase is a primary phase, and the presence of hematite in one section suggests that it might have been the ore mineral used. The presence of resistate grains of chromite and quartz suggest that local sand or sandstone was part of the flux, while the high lime content suggests that limestone was added as well.

The absence of any modal or normative wüstite makes these slags unusual compared to other medieval and Roman iron-smelting sites.

Acknowledgements

We would like to thank the Department of Geological Sciences for providing time on the Cameca (SX-50) microprobe in the Electron Microscope Center of the University of South Carolina. Mark Wieland assisted with obtaining the backscatter images, with the calibration, and with the analyses of the various minerals and glass, while Donggao Zhou helped to maintain the equipment. The samples for ^{14}C dating were analysed as follows: AA samples – NSF Arizona AMS Facility, University of Arizona (Tucson); the GX sample – Geochron Laboratories (Cambridge, Massachusetts).

References

Akyürek, B., Akbaş, B. & Dağer, Z. 1988. *1:100,000 Scale Geological Map of Turkey Series, Çankırı – E16 Sheet*. General Directorate of Mineral Research and Exploration (MTA) Publications, Ankara.

Bosi, F., Haalenius, U. & Skogby, H. 2008. Stoichiometry of synthetic ulvöspinel single crystals. *American Mineralogist* **93**, 1312–1316.

Budanur, G. 1977. *MTA Enstitüsünce Bilinen Türkiye Yeraltı Kaynakları Envanteri (Inventory of Turkish Subsurface Resources Known to the MTA Institute)*. Mineral Research and Exploration Institute of Turkey, Publication no. **168**, Ankara [in Turkish, unpublished].

Coulant, Ettore 1907. *Note sur deux permis de recherches pour cuivre appurtenant à S.E. Fuat Bey et Dicran Balıkçian dans le vilâyet de Kastamonu*. Mineral Research and Exploration Institute of Turkey, Ankara, Report no. **323**.

De Jesus, P.S. 1973. A la recherche du metallurgiste ancien. *Archeologia* (Paris) **68**, 70–72.

De Jesus, P.S. 1978. Metal resources of ancient Anatolia. *Anatolian Studies* **28**, 97–102.

De Jesus, P.S. 1980. *The Development of Prehistoric Mining and Metallurgy in Anatolia*. British Archaeological Reports, International Series **74**.

Deer, W.A., Howie, R.A. & Zussman, J. 1962b. *Rock-forming Minerals, v. 2, Chain Silicates.* John Wiley, New York.

Deer, W.A., Howie, R.A. & Zussman, J. 1962e. *Rock-forming Minerals, v. 5, Non-Silicates.* John Wiley, New York.

Hansen, M. 1958. *Constitution of Binary Alloys* (2nd ed). McGraw-Hill, New York.

Imber, C. 2002. *The Ottoman Empire, 1300–1650.* Palgrave Macmillan, New York.

Josephson, G.W., Sillers Jr., F. & Runner, D.G. 1949. *Iron Blast-Furnace Slag.* United States Bureau of Mines, Bulletin 479, Washington, D.C.

Lee, A.R. 1974. *Blastfurnace and Steel Slag.* Edward Arnold, London.

Maucher, 1937. *Çankırı ve Tosya Tetkikine Ait Raporlar (Reports of the Çankırı and Tosya Investigation)*. Mineral Research and Exploration Institute of Turkey, Ankara Report no. **340** [in Turkish, unpublished].

Morton, G.R. & Wingrove, J. 1969. Constitution of bloomery slags: Part I: Roman. *Journal of the Iron and Steel Institute* **207,** 1556-1564.

Morton, G.R. & Wingrove, J. 1972. Constitution of bloomery slags: Part II: Medieval. *Journal of the Iron and Steel Institute* **210**, 478–488.

MTA, 1972. *Lead, Copper and Zinc Deposits of Turkey*. Mineral Research and Exploration Institute of Turkey, Publication no. **133**, Ankara.

Nowak. 1927. *Çankırı Demir Madeni* (*Iron Deposits of Çankırı*). Mineral Research and Exploration Institute of Turkey, Ankara, Report no. **440** [in Turkish, unpublished].

Partington, J.R. 1939. *A Test-Book of Inorganic Chemistry* (5th ed). Macmillan, London.

Pouchou, J.-L. & Pichoir, F. 1991. Quantitative analysis of homogeneous or stratified microvolumes applying the model 'PAP'. *In*: Heinrich, K.F.J. & Newbury, D.E. (eds), *Electron Probe Quantitation*. Plenum, New York, 31–75.

Rehren, T., Charlton, M., Chirikure, S., Humphris, J., Ige, A. & Veldhuijzen, H.A. 2007. Decisions set in slag: the human factor in African iron smelting. *In:* La Niece, S., Hook, D. & Craddock, P (eds), *Metals and Mines: Studies in Archaeometallurgy.* Archetype, London, 211–218.

Ryan, C.W. 1957. *A Guide to the Known Minerals of Turkey*. Mineral Research and Exploration Institute of Turkey, Ankara.

Schairer, J.F. 1942. The system CaO-FeO-Al_2O_3-SiO_2: I., Results of quenching experiments on five joins. *Journal of the American Ceramic Society* **25**, 241–274.

Seeliger, T.C., Pernicka, E., Wagner, G.A., Begemann, F., Schmitt-Strecker, S., Eibner, C., Öztunali, Ö. & Baranyi, I. 1985. Archæometallurgische Untersuchungen in Nord- und Ostanatolien. *Jahrbuch des Römisch-Germanischen Zentralmuseums* **32**, 597–659.

Uğuz, M.F., Sevin, M. & Duru, M. (compilers). 2002. *1:500,000 Scale Geological Maps of Turkey, no: **3**, Sinop Sheet*. General Directorate of Mineral Research and Exploration (MTA) Publications, Ankara.

Wertime, T.A. 1980. The pyrotechnologic background. *In:* Wertime, T.A. & Muhly, J.D. (eds), *The Coming of the Age of Iron.* Yale University Press, New Haven, 1–24.

A Note: Appendix materials will only be found in the electronic version.

Appendix A

Table A1. Composition of Metallic Iron.

Sample	spot	wt	Si	Ti	Al	Fe	Mn	Mg	Ca	Na	K	P	Ba	Cr	Total
TK97–07A1	14	%	1.81	0.07	0.01	98.03	0.06	0.00	0.04	0.01	0.04	0.13	0.06	0.14	100.00
TK97–07A1	15	%	0.00	0.07	0.00	102.20	0.12	0.00	0.05	0.01	0.05	0.05	0.07	0.13	102.76
TK97–07A1	16	%	0.00	0.05	0.02	102.33	0.09	0.01	0.05	0.01	0.05	0.14	0.08	0.17	103.00
TK97–07A1	17	%	0.01	0.09	0.01	102.48	0.10	0.00	0.06	0.00	0.05	0.17	0.23	0.14	103.12
TK97–07A4	34	%	0.00	0.68	0.00	99.09	0.07	0.04	0.05	0.02	0.04	0.37	0.02	0.17	100.56
TK97–07A4	35	%	0.00	0.13	0.03	100.94	0.07	0.01	0.08	0.01	0.06	0.07	0.06	0.17	101.61
TK97–07A7	53	%	0.00	0.41	0.24	98.50	0.10	0.08	0.06	0.01	0.05	0.07	0.09	0.20	99.82
TK99–10C3	65	%	0.01	0.10	0.00	100.89	0.07	0.00	0.06	0.00	0.05	0.21	0.21	0.13	101.72
TK99–10C3	66	%	0.00	0.07	0.01	99.10	0.08	0.01	0.05	0.00	0.06	0.22	0.04	0.15	99.77
TK99–10C3	67	%	0.01	0.07	0.01	98.96	0.07	0.00	0.04	0.00	0.05	0.10	0.19	0.15	99.65
TK99–10C3	68	%	0.00	0.09	0.01	99.02	0.08	0.01	0.06	0.03	0.06	0.16	0.10	0.14	99.75
TK97–06B2	9	%	0.00	0.09	0.01	102.60	0.13	0.02	0.12	0.05	0.07	0.06	0.36	0.25	103.77
TK97–06B2	10	%	0.00	0.11	0.00	102.10	0.15	0.03	0.12	0.03	0.06	0.04	0.38	0.24	103.26
TK97–06B3	18	%	0.00	0.09	0.01	101.43	0.13	0.03	0.10	0.04	0.07	0.06	0.34	0.30	102.58
TK97–06B3	19	%	0.22	0.05	0.01	92.22	0.39	0.04	0.11	0.03	0.07	0.04	0.32	2.71	96.19
TK99–10B2	38	%	0.00	0.04	0.01	99.31	0.12	0.02	0.08	0.04	0.08	0.17	0.31	0.23	100.41
TK99–10B2	39	%	0.00	0.09	0.01	100.78	0.15	0.04	0.09	0.03	0.08	0.16	0.41	0.23	102.09
TK99–10A9	103	%	0.00	0.14	0.01	98.99	0.14	0.01	0.17	0.03	0.07	0.04	0.41	0.23	100.23
TK99–10A9	104	%	0.00	0.15	0.01	99.29	0.17	0.04	0.17	0.03	0.07	0.05	0.26	0.25	100.49
TK99–08A3	43	%	0.07	0.49	0.12	98.31	0.01	0.04	0.07	0.04	0.02	0.00	0.02	0.01	99.23
TK99–08A3	44	%	0.03	0.18	0.01	101.36	0.00	0.01	0.06	0.01	0.02	0.02	0.00	0.02	101.71
TK99–04C4	20	%	0.03	0.04	0.00	99.87	0.01	0.00	0.00	0.04	0.00	0.15	0.07	0.00	100.22
TK99–04C4	21	%	0.03	0.01	0.01	99.78	0.00	0.00	0.01	0.03	0.00	0.08	0.00	0.02	99.97
TK99–04C4	22	%	0.02	0.04	0.00	100.19	0.00	0.00	0.00	0.03	0.01	0.60	0.00	0.01	100.89
TK99–04C5	30	%	0.02	0.00	0.00	100.05	0.03	0.00	0.00	0.00	0.00	0.13	0.00	0.02	100.25
TK97–06C2	50	%	1.17	0.00	0.01	96.56	0.07	0.00	0.00	0.00	0.02	0.20	0.00	0.60	98.62
TK97–06C2	53	%	1.29	0.02	0.00	97.40	0.01	0.01	0.00	0.03	0.00	0.08	0.08	0.47	99.40
TK97–06C2	55	%	1.27	0.03	0.01	96.25	0.00	0.00	0.00	0.02	0.00	0.13	0.06	0.47	98.22
TK99–03A3	75	%	0.02	0.08	0.00	99.49	0.05	0.00	0.06	0.06	0.02	1.70	0.00	0.03	101.51
TK99–03A3	76	%	0.04	0.04	0.00	99.07	0.04	0.00	0.14	0.05	0.02	1.27	0.00	0.00	100.68
TK99–04A3	104	%	0.03	0.02	0.00	96.75	0.03	0.01	0.01	0.00	0.00	0.09	0.00	0.07	97.01
average	0	%	0.20	0.11	0.02	99.46	0.08	0.02	0.06	0.02	0.04	0.22	0.13	0.25	100.60

Table A2. Additional Iron Slag Locations of the Yapraklı Area.

Sites reported but not visited in this study:

(de Jesus 1980, p. 241–245)
Ahmet Burhan
Damlu Yurt Deresi
Eyriceova Mevkii
Kıyaltı Mevkii
Mehmet Takmen Tar.
Papurun Kaşı
Yanyaylası Mevkii

(Seeliger *et al.* 1985, p. 601)
Papazın Kaşı Tepe
Ovacık Yaylası
Ak Gedikin Kaş, Arta Yere
Kavak Yayla
Kapaklı Kaş

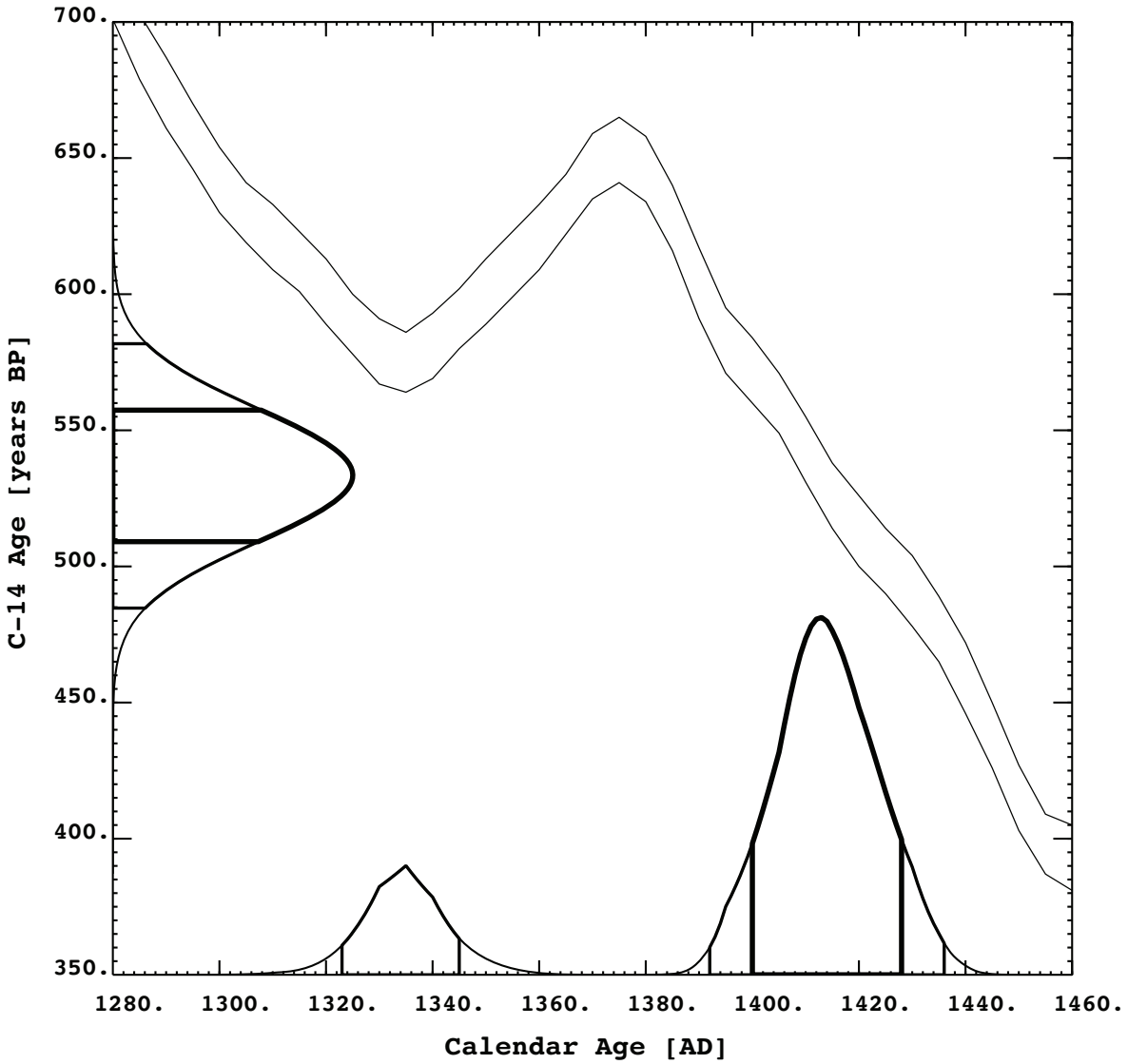

Figure A1. Diagram showing measured C-14 ages versus calendar ages.

Appendix B

Table B1. Composition of Metallic Iron.

Sample	spot	wt	Si	Ti	Al	Fe	Mn	Mg	Ca	Na	K	P	Ba	Cr	Total
97–07A1	14	%	1.81	0.07	0.01	98.03	0.06	0.00	0.04	0.01	0.04	0.13	0.06	0.14	100.00
97–07A1	15	%	0.00	0.07	0.00	102.20	0.12	0.00	0.05	0.01	0.05	0.05	0.07	0.13	102.76
97–07A1	16	%	0.00	0.05	0.02	102.33	0.09	0.01	0.05	0.01	0.05	0.14	0.08	0.17	103.00
97–07A1	17	%	0.01	0.09	0.01	102.48	0.10	0.00	0.06	0.00	0.05	0.17	0.23	0.14	103.12
97–07A4	34	%	0.00	0.68	0.00	99.09	0.07	0.04	0.05	0.02	0.04	0.37	0.02	0.17	100.56
97–07A4	35	%	0.00	0.13	0.03	100.94	0.07	0.01	0.08	0.01	0.06	0.07	0.06	0.17	101.61
97–07A7	53	%	0.00	0.41	0.24	98.50	0.10	0.08	0.06	0.01	0.05	0.07	0.09	0.20	99.82
99–10C3	65	%	0.01	0.10	0.00	100.89	0.07	0.00	0.06	0.00	0.05	0.21	0.21	0.13	101.72
99–10C3	66	%	0.00	0.07	0.01	99.10	0.08	0.01	0.05	0.00	0.06	0.22	0.04	0.15	99.77
99–10C3	67	%	0.01	0.07	0.01	98.96	0.07	0.00	0.04	0.00	0.05	0.10	0.19	0.15	99.65
99–10C3	68	%	0.00	0.09	0.01	99.02	0.08	0.01	0.06	0.03	0.06	0.16	0.10	0.14	99.75
99–06B2	9	%	0.00	0.09	0.01	102.60	0.13	0.02	0.12	0.05	0.07	0.06	0.36	0.25	103.77
99–06B2	10	%	0.00	0.11	0.00	102.10	0.15	0.03	0.12	0.03	0.06	0.04	0.38	0.24	103.26
99–06B3	18	%	0.00	0.09	0.01	101.43	0.13	0.03	0.10	0.04	0.07	0.06	0.34	0.30	102.58
99–06B3	19	%	0.22	0.05	0.01	92.22	0.39	0.04	0.11	0.03	0.07	0.04	0.32	2.71	96.19
99–10B2	38	%	0.00	0.04	0.01	99.31	0.12	0.02	0.08	0.04	0.08	0.17	0.31	0.23	100.41
99–10B2	39	%	0.00	0.09	0.01	100.78	0.15	0.04	0.09	0.03	0.08	0.16	0.41	0.23	102.09
99–10A9	103	%	0.00	0.14	0.01	98.99	0.14	0.01	0.17	0.03	0.07	0.04	0.41	0.23	100.23
99–10A9	104	%	0.00	0.15	0.01	99.29	0.17	0.04	0.17	0.03	0.07	0.05	0.26	0.25	100.49
99–08A3	43	%	0.07	0.49	0.12	98.31	0.01	0.04	0.07	0.04	0.02	0.00	0.02	0.01	99.23
99–08A3	44	%	0.03	0.18	0.01	101.36	0.00	0.01	0.06	0.01	0.02	0.02	0.00	0.02	101.71
99–04C4	20	%	0.03	0.04	0.00	99.87	0.01	0.00	0.00	0.04	0.00	0.15	0.07	0.00	100.22
99–04C4	21	%	0.03	0.01	0.01	99.78	0.00	0.00	0.01	0.03	0.00	0.08	0.00	0.02	99.97
99–04C4	22	%	0.02	0.04	0.00	100.19	0.00	0.00	0.00	0.03	0.01	0.60	0.00	0.01	100.89
99–04C5	30	%	0.02	0.00	0.00	100.05	0.03	0.00	0.00	0.00	0.00	0.13	0.00	0.02	100.25
99–06C2	50	%	1.17	0.00	0.01	96.56	0.07	0.00	0.00	0.00	0.02	0.20	0.00	0.60	98.62
99–06C2	53	%	1.29	0.02	0.00	97.40	0.01	0.01	0.00	0	.03	0.00	0.08	0.08	0.47
99.40															
99–06C2	55	%	1.27	0.03	0.01	96.25	0.00	0.00	0.00	0.02	0.00	0.13	0.06	0.47	98.22
99–03A3	75	%	0.02	0.08	0.00	99.49	0.05	0.00	0.06	0.06	0.02	1.70	0.00	0.03	101.51
99–03A3	76	%	0.04	0.04	0.00	99.07	0.04	0.00	0.14	0.05	0.02	1.27	0.00	0.00	100.68
99–04A3	104	%	0.03	0.02	0.00	96.75	0.03	0.01	0.01	0.00	0.00	0.09	0.00	0.07	97.01
average	0	%	0.20	0.11	0.02	99.46	0.08	0.02	0.06	0.02	0.04	0.22	0.13	0.25	100.60

Table B2. Composition of Plagioclase (Labradorite-Bytownite).

Sample	spot	wt	SiO_2	TiO_2	Al_2O_3	FeO	MnO	MgO	CaO	Na_2O	K_2O	P_2O_5	BaO	Cr_2O_3	Total
97–07A3	28.	%	46.77	0.05	28.06	5.41	0.00	0.15	13.17	1.92	0.61	0.03	0.00	0.00	96.16
97–07A3	29.	%	48.90	0.05	29.58	0.93	0.00	0.15	14.41	2.05	1.07	0.00	0.00	0.00	97.13
97–07A3	32.	%	48.84	0.10	29.60	0.41	0.00	0.27	15.00	2.00	0.87	0.01	0.00	0.00	97.08
97–07A6	48.	%	48.29	0.00	29.72	0.49	0.00	0.00	15.39	1.42	1.28	0.00	0.00	0.00	96.60
97–07A6	49.	%	48.22	0.10	29.54	0.85	0.00	0.29	15.54	1.43	1.08	0.02	0.00	0.00	97.07
99–06B1	3.	%	49.67	0.14	29.71	1.62	0.00	0.30	14.04	2.40	0.94	0.03	0.00	0.02	98.88
99–06B1	4.	%	49.32	0.03	30.24	0.84	0.00	0.31	14.96	2.17	0.74	0.02	0.03	0.01	98.65
99–06B3	22.	%	50.27	0.11	28.73	0.90	0.00	0.30	13.85	2.38	1.41	0.06	0.03	0.03	98.06
99–06B3	23.	%	50.38	0.17	28.98	0.85	0.02	0.20	13.57	2.42	1.47	0.02	0.03	0.01	98.12
99–06B3	24.	%	50.83	0.18	28.04	1.22	0.03	0.33	13.58	2.48	1.55	0.02	0.08	0.02	98.34
99–06B3	25.	%	52.11	0.16	26.86	1.24	0.00	0.32	12.35	2.57	2.19	0.02	0.10	0.02	97.93
99–06B4	27.	%	50.40	0.13	27.90	1.37	0.05	0.33	14.07	2.27	1.52	0.05	0.12	0.01	98.21
99–06B4	28.	%	50.28	0.09	28.70	1.24	0.03	0.25	14.21	2.19	1.35	0.02	0.17	0.02	98.53
99–04B2	3.	%	51.59	0.22	28.52	1.13	0.02	0.87	15.19	2.11	0.74	0.04	0.02	0.03	100.47
99–04B2	7.	%	50.85	1.74	24.47	2.92	0.10	2.01	14.95	1.83	0.77	0.12	0.05	0.12	99.95
99–08A5	34.	%	48.99	0.17	31.23	1.62	0.01	0.19	15.86	1.74	1.16	0.00	0.00	0.05	101.01
99–08A5	35.	%	49.58	0.00	31.09	1.64	0.01	0.15	15.40	1.93	1.29	0.00	0.06	0.00	101.15
99–08A5	36.	%	50.25	0.13	29.79	1.90	0.03	0.23	14.59	2.07	1.58	0.03	0.00	0.00	100.58
99–10A2	70.	%	49.88	0.06	28.08	1.29	0.01	0.14	14.13	2.28	1.21	0.02	0.17	0.04	97.30
99–10A2	71.	%	49.99	0.16	28.40	1.50	0.02	0.17	14.27	2.27	1.04	0.01	0.09	0.02	97.95
99–10A4	80.	%	49.49	0.25	28.25	2.08	0.02	0.19	13.91	2.23	0.97	0.01	0.09	0.02	97.52
99–10A4	81.	%	50.18	0.06	28.47	1.33	0.01	0.19	14.13	2.34	0.93	0.01	0.13	0.00	97.78
average	0	%	49.78	0.19	28.82	1.49	0.02	0.33	14.39	2.11	1.17	0.03	0.05	0.02	98.39
Ideal–An70	%	50.54	.0	31.70	.0	.0	.0	14.36	3.40	.0	.0	.0	.0	100.00	

Table B3. Composition of Leucite.

Sample	spot	wt	SiO_2	TiO_2	Al_2O_3	FeO	MnO	MgO	CaO	Na_2O	K_2O	P_2O_5	BaO	Cr_2O_3	Total
97–07A5	40	%	54.80	0.11	21.97	0.04	0.00	0.00	0.00	0.57	19.21	0.03	0.00	0.00	96.71
97–07A5	41	%	55.24	0.09	21.63	0.00	0.00	0.00	0.00	0.62	19.21	0.00	0.00	0.00	96.79
97–07A5	42	%	55.01	0.04	22.31	0.07	0.00	0.00	0.00	0.70	18.96	0.00	0.00	0.00	97.09
97–07A5	43	%	55.01	0.13	21.85	0.00	0.00	0.01	0.00	0.67	19.10	0.00	0.00	0.00	96.76
average	0	%	55.01	0.09	21.94	0.03	0.00	0.00	0.00	0.64	19.12	0.01	0.00	0.00	96.84
Ideal	0	%	55.06	.0	23.36	.0	.0	.0	.0	.0	21.58	.0	.0	.0	100.00

Table B4. Composition of Titanaugite.

Sample	spot	wt	SiO_2	TiO_2	Al_2O_3	FeO	MnO	MgO	CaO	Na_2O	K_2O	P_2O_5	BaO	Cr_2O_3	Total
97–07A3	30	%	45.53	3.59	10.00	16.89	0.20	1.03	15.16	1.50	3.12	0.55	0.00	0.00	97.55
97–07A3	33	%	45.28	3.54	6.88	8.11	0.23	11.81	20.73	0.17	0.00	0.08	0.00	0.88	97.70
97–07A5	44	%	40.87	4.44	8.95	13.17	0.25	7.41	22.49	0.04	0.01	0.55	0.00	0.00	98.18
97–07A5	45	%	41.43	3.78	8.69	13.95	0.23	6.82	22.15	0.06	0.01	0.39	0.00	0.00	97.52
97–07A5	46	%	41.73	4.05	8.76	13.07	0.20	7.54	22.50	0.07	0.00	0.44	0.00	0.00	98.35
97–07A5	47	%	41.75	3.59	8.13	16.20	0.32	5.83	22.00	0.09	0.01	0.10	0.00	0.00	98.01
99–06B1	5	%	47.21	2.46	6.03	12.39	0.40	13.66	16.73	0.20	0.14	0.11	0.14	0.23	99.68
99–06B1	6	%	47.73	2.00	5.36	14.35	0.47	14.21	14.82	0.18	0.13	0.11	0.07	0.25	99.69
99–06B4	29	%	41.84	4.75	8.85	15.14	0.23	6.50	21.06	0.12	0.04	0.21	0.16	0.13	99.01
99–06B4	30	%	41.66	5.09	8.73	15.75	0.31	6.12	21.19	0.16	0.03	0.28	0.08	0.11	99.51
99–03B2	46	%	42.66	3.21	7.91	18.74	0.39	6.41	17.21	0.23	0.36	0.21	0.14	0.13	97.59
99–03B2	47	%	41.77	3.34	7.39	20.81	0.40	5.77	16.90	0.20	0.21	0.16	0.05	0.26	97.26
99–03B2	50	%	42.73	3.58	9.07	19.17	0.36	5.12	16.11	0.39	0.94	0.19	0.11	0.18	97.96
99–03B2	51	%	41.66	3.89	8.15	19.17	0.30	5.97	17.74	0.16	0.34	0.23	0.07	0.23	97.92
99–10A4	92	%	46.13	3.31	11.03	17.92	0.31	1.34	15.76	0.77	1.28	0.23	0.18	0.09	98.35
99–10A4	93	%	46.70	2.87	10.61	17.47	0.35	3.31	13.81	0.43	2.16	0.25	0.11	0.10	98.16
average	0	%	43.54	3.59	8.41	15.77	0.31	6.80	18.52	0.30	0.55	0.26	0.07	0.16	98.28
2	0	%	47.11	3.75	3.00	15.56	.0	16.85	13.54	0.22	0.02	.0	.0	.0	99.96
3	0	%	40.28	3.85	10.30	12.73	.0	7.78	23.57	0.36	.0	.0	.0	.0	99.06

2) titanaugite, basalt, Hiva Oa, Marquesas Is.
3) titanaugite, melilite-nepheline dolerite, Scawt Hill Co. Antrim. Fe_2O_3 converted to FeO(from Deer et al. 1963b, p. 123)

Table B5. Composition of Ulvöspinel*.

Sample	spot	wt	SiO_2	TiO_2	Al_2O_3	FeO	MnO	MgO	CaO	Na_2O	K_2O	P_2O_5	BaO	Cr_2O_3	Total
99–06B4	31	%	0.00	28.12	3.32	60.71	0.71	0.55	0.25	0.02	0.11	0.08	0.31	3.16	97.33
99–10A2	74	%	0.50	27.07	3.53	60.32	0.53	1.13	0.29	0.02	0.16	0.06	0.40	1.77	95.77
99–10A4	82	%	0.00	24.31	3.52	58.00	0.56	1.20	0.27	0.04	0.08	0.08	0.43	6.86	95.33
99–10A4	84	%	0.00	26.93	4.11	60.63	0.59	0.50	0.29	0.04	0.08	0.06	0.33	2.55	96.11
99–10A4	87	%	0.00	26.22	3.54	59.58	0.55	1.29	0.27	0.01	0.07	0.06	0.25	4.09	95.92
99–08A4	27	%	0.24	26.59	5.47	62.34	0.53	0.24	0.10	0.01	0.02	0.00	0.00	0.49	96.02
99–04C3	17	%	0.36	27.77	5.48	58.09	0.42	1.60	0.24	0.01	0.07	0.00	0.00	1.87	95.93
99–04C1	40	%	0.37	22.64	6.95	52.76	0.17	2.53	0.25	0.00	0.05	0.00	0.00	8.48	94.21
99–04C1	41	%	0.30	23.34	7.57	54.69	0.25	1.91	0.32	0.00	0.06	0.00	0.00	6.06	94.50
average	0	%	0.20	25.89	4.83	58.57	0.48	1.22	0.25	0.02	0.08	0.04	0.19	3.93	95.68
Ideal	0	%	0.00	35.73	0.00	64.27	0.00	0.00	0.00	0.00	0.00	0.00	0.00	0.00	100.00
8	0	%	0.33	26.76	2.31	64.29	0.61	1.93	0.59	.0	.0	.0	.0	0.38	97.48

*Most ulvöspinel is in solid solution with magnetite.
8 - Titanomagnetite, teschenite, Black Jack sill, Gunnnedah, NSW, Australia Fe_2O_3 recalculated as FeO (Deer *et al.* 1962e, p. 73)

Table B6a. Composition of Fayalite* – Fa66.

Sample	spot	wt	SiO_2	TiO_2	Al_2O_3	FeO	MnO	MgO	CaO	Na_2O	K_2O	P_2O_5	BaO	Cr_2O_3	Total
97–07A3	31	%	32.93	0.12	0.00	45.05	0.56	19.62	0.84	0.01	0.00	0.08	0.00	0.00	99.21
99–06B1	8	%	31.57	0.19	0.08	55.00	1.33	10.90	1.14	0.02	0.10	0.10	0.14	0.13	100.70
99–06B3	26	%	34.76	0.22	0.45	41.34	0.80	22.59	0.75	0.05	0.25	0.14	0.16	0.14	101.65
99–04C1	39	%	31.37	0.34	0.16	55.90	0.61	10.64	0.78	0.01	0.06	0.03	0.17	0.04	100.11
99–04C2	37	%	31.82	0.34	0.11	54.05	0.59	12.49	0.77	0.00	0.03	0.05	0.00	0.01	100.24
99–04C2	38	%	31.57	0.25	0.12	55.37	0.63	11.49	0.72	0.02	0.00	0.02	0.03	0.05	100.28
average	0	%	32.34	0.24	0.15	51.12	0.75	14.62	0.84	0.02	0.07	0.07	0.08	0.06	100.37
Fa66	0	%	32.95	.0	.0	52.01	.0	15.03	.0	.0	.0	.0	.0	.0	99.99

*values of CaO greater than 0.9 % and values of K2O greater than 0.5 % suggest the presence of admixed glass.

Table B6b. Composition of Fayalite* – Fa88.

Sample	spot	wt	SiO_2	TiO_2	Al_2O_3	FeO	MnO	MgO	CaO	Na_2O	K_2O	P_2O_5	BaO	Cr_2O_3	Total
99–06B1	7	%	30.02	0.26	0.19	57.37	1.68	7.10	2.60	0.01	0.12	0.91	0.09	0.13	100.50
99–08A2	15	%	29.60	0.34	0.06	64.71	0.74	2.90	0.89	0.04	0.01	0.03	0.17	0.01	99.50
99–08A2	16	%	29.90	0.38	0.10	64.06	0.79	4.98	0.65	0.01	0.01	0.17	0.07	0.00	101.12
99–08A2	19	%	30.13	0.41	0.08	63.51	0.76	5.07	0.59	0.02	0.00	0.10	0.00	0.00	100.69
99–08A4	25	%	29.23	0.35	0.11	66.12	0.60	2.33	0.06	0.00	0.01	0.13	0.00	0.00	98.96
99–08A4	26	%	29.73	0.26	0.12	64.20	0.92	3.67	0.09	0.00	0.00	0.19	0.00	0.02	99.19
99–10A4	88	%	34.97	0.52	3.42	50.12	0.81	6.09	2.03	0.36	0.76	0.10	0.17	0.10	99.43
average	0	%	30.51	0.36	0.58	61.44	0.90	4.59	0.98	0.06	0.13	0.23	0.07	0.04	99.91
Fa88	0	%	30.62	.0	.0	64.44	.0	4.93	.0	.0	.0	.0	.0	.0	99.99

*values of CaO greater than 0.9 % and values of K2O greater than 0.5% suggest the presence of admixed glass.

Table B7. Composition of Hematite*

Sample	spot	wt	SiO_2	TiO_2	Al_2O_3	FeO	MnO	MgO	CaO	Na_2O	K_2O	P_2O_5	BaO	Cr_2O_3	Total
97–07A1	18	%	0.16	0.10	0.07	89.69	0.04	0.00	0.06	0.00	0.03	0.08	0.00	0.05	90.28
97–07A1	20	%	0.40	0.06	0.03	87.19	0.06	0.00	0.12	0.02	0.04	0.20	0.00	0.24	88.35
97–07A1	21	%	0.18	0.06	0.02	88.70	0.04	0.00	0.08	0.03	0.05	0.05	0.00	0.03	89.25
99–09B3	20	%	0.37	0.10	0.02	89.03	0.09	0.00	0.13	0.00	0.07	0.28	0.24	0.18	90.50
97–09B3	21	%	0.28	0.10	0.01	90.63	0.12	0.01	0.12	0.03	0.07	0.09	0.23	0.21	91.89
99–04B1	1	%	0.09	0.14	0.02	88.09	0.04	0.02	0.12	0.20	0.00	0.21	0.15	0.09	89.19
99–10A5	94	%	0.18	2.44	0.50	86.33	0.43	0.24	0.09	0.01	0.06	0.06	0.21	0.20	90.76
average	0	%	0.24	0.43	0.10	88.52	0.12	0.04	0.10	0.04	0.05	0.14	0.12	0.14	90.03
ideal	0	%	.0	.0	.0	89.98	.0	.0	.0	.0	.0	.0	.0	.0	89.98

*Total iron expressed as FeO.

Table B8. Composition of Magnesiochromite.

Sample	spot	wt	SiO_2	TiO_2	Al_2O_3	Cr_2O_3	FeO	MnO	MgO	CaO	Na_2O	K_2O	P_2O_5	BaO	Total
99–06B2	12	%	0.00	0.26	7.53	63.52	20.72	1.28	7.97	0.12	0.02	0.04	0.04	0.23	101.73
99–10A7	100	%	0.00	0.22	5.66	61.67	24.34	0.51	8.06	0.08	0.03	0.05	0.01	0.17	100.81
99–08A1	1	%	0.01	0.09	6.23	60.15	25.79	0.00	6.78	0.01	0.01	0.00	0.00	0.17	99.24
99–08A2	12	%	0.03	0.27	7.12	59.86	24.34	0.00	7.49	0.00	0.00	0.00	0.03	0.00	99.14
99–03A6	88	%	0.02	0.04	12.26	57.88	19.26	0.00	10.78	0.03	0.03	0.01	0.05	0.03	100.38
99–03B2	42	%	0.00	0.18	6.64	55.44	29.11	0.61	6.25	0.07	0.03	0.06	0.04	0.26	98.66
99–03B2	43	%	0.00	0.28	11.51	54.56	23.80	0.41	7.56	0.08	0.02	0.06	0.06	0.24	98.57
99–10A3	79	%	0.00	0.03	15.67	54.21	20.71	0.45	9.42	0.07	0.04	0.05	0.02	0.15	100.81
99–03A3	74	%	0.03	0.27	17.35	53.84	17.26	0.00	11.61	0.03	0.07	0.00	0.00	0.30	100.78
99–03A1	58	%	0.05	0.10	16.01	53.48	20.20	0.00	9.56	0.08	0.02	0.01	0.00	0.19	99.71
99–08A2	13	%	0.04	0.36	15.11	53.19	22.54	0.00	8.73	0.02	0.02	0.00	0.01	0.00	100.03
99–10A3	78	%	0.00	0.09	15.14	53.00	24.03	0.58	7.28	0.08	0.03	0.03	0.03	0.26	100.56
99–08A2	11	%	0.32	0.34	15.72	51.61	24.27	0.00	8.00	0.03	0.00	0.04	0.00	0.02	100.36
99–08A1	3	%	0.01	0.26	18.07	50.97	19.70	0.00	10.83	0.00	0.02	0.01	0.03	0.00	99.90
99–08A1	4	%	0.01	0.26	18.38	50.55	19.95	0.00	10.70	0.01	0.00	0.00	0.01	0.00	99.86
99–10C6	78	%	0.22	0.11	20.07	48.14	20.33	0.29	9.88	0.08	0.00	0.01	0.01	0.00	99.14
99–10C2	62	%	0.00	0.07	22.20	47.65	16.52	0.26	12.85	0.00	0.00	0.00	0.03	0.00	99.58
99–10C2	61	%	0.00	0.01	22.16	47.22	16.31	0.26	12.77	0.00	0.01	0.00	0.01	0.00	98.75
99–10C6	77	%	0.20	0.13	22.30	46.27	20.16	0.28	10.19	0.07	0.00	0.00	0.00	0.00	99.61
99–03B2	48	%	0.00	0.39	20.62	44.54	23.22	0.37	7.81	0.13	0.04	0.06	0.04	0.13	97.34
99–08A2	18	%	0.03	0.07	25.46	43.64	18.36	0.00	12.69	0.01	0.01	0.00	0.00	0.00	100.27
99–08A2	18	%	0.03	0.07	25.46	43.64	18.36	0.00	12.69	0.01	0.01	0.00	0.00	0.00	100.27
99–04A4	111	%	0.07	0.07	25.26	43.04	18.23	0.00	12.25	0.04	0.00	0.00	0.00	0.01	98.95
99–03A1	57	%	0.01	0.15	27.69	40.98	18.92	0.00	12.02	0.05	0.02	0.01	0.01	0.07	99.92
99–04C2	36	%	0.00	0.36	27.01	38.60	23.18	0.00	11.06	0.00	0.02	0.00	0.00	0.04	100.28
99–03A5	86	%	0.09	0.13	33.89	36.89	13.21	0.00	15.40	0.08	0.03	0.02	0.00	0.08	99.82
99–03A1	59	%	0.02	0.17	35.36	35.22	14.69	0.00	15.56	0.03	0.02	0.02	0.04	0.00	101.13
99–03A3	73	%	0.05	0.20	36.42	32.46	16.35	0.00	14.41	0.05	0.06	0.02	0.04	0.00	100.05
average	0	%	0.04	0.18	19.01	49.36	20.49	0.19	10.38	0.04	0.02	0.02	0.02	0.08	99.84
5	0	%	.0	0.69	13.36	52.77	21.78	0.20	10.31	0.28	.0	.0	.0	.0	99.39

5 – chromite, Kolhan Govt. Estate, Singhbhum district, Bihar, India Fe_2O_3 recalculated as FeO (Deer *et al.* 1962e p. 79).

Table B9. Composition of Quartz.

Sample	spot	wt	SiO_2	TiO_2	Al_2O_3	FeO	MnO	MgO	CaO	Na_2O	K_2O	P_2O_5	BaO	Cr_2O_3	Total
97–07A2	26	%	97.78	0.00	0.26	0.00	0.00	0.00	0.00	0.00	0.00	0.00	0.00	0.00	98.03
97–07A2	27	%	92.72	0.00	3.11	0.31	0.00	0.01	0.00	0.33	1.92	0.00	0.00	0.00	98.41
97–07A4	38	%	89.41	0.00	2.56	1.68	0.00	0.20	0.74	0.22	1.33	0.60	0.00	0.00	96.73
97–07A4	39	%	92.32	0.00	0.93	0.36	0.00	0.13	1.81	0.23	0.32	0.00	0.00	0.00	96.10
99–10C5	73	%	98.11	0.00	0.04	0.00	0.00	0.00	0.00	0.00	0.00	0.00	0.00	0.00	98.15
99–10C5	74	%	97.29	0.00	0.06	0.00	0.00	0.00	0.00	0.00	0.00	0.00	0.00	0.00	97.35
99–06B1	1	%	98.20	0.00	0.14	0.15	0.00	0.05	0.01	0.00	0.10	0.00	0.00	0.00	98.66
99–06B1	2	%	98.25	0.00	0.27	0.23	0.00	0.04	0.04	0.00	0.06	0.00	0.17	0.00	99.06
99–06B2	15	%	96.75	0.00	1.14	0.35	0.00	0.24	0.01	0.02	0.23	0.01	0.08	0.00	98.82
99–10A4	90	%	96.77	0.00	0.45	0.18	0.00	0.01	0.06	0.06	0.23	0.00	0.00	0.00	97.77
99–10A4	91	%	97.56	0.00	0.02	0.49	0.00	0.00	0.02	0.00	0.03	0.02	0.00	0.00	98.14
99–10A8	101	%	97.97	0.00	0.04	0.14	0.00	0.00	0.01	0.02	0.01	0.00	0.00	0.00	98.19
99–10A8	102	%	97.97	0.00	0.01	0.15	0.00	0.00	0.00	0.00	0.01	0.00	0.10	0.00	98.25
99–08A1	5	%	99.39	0.00	0.16	0.17	0.02	0.03	0.02	0.04	0.10	0.01	0.00	0.01	99.93
99–08A1	6	%	99.52	0.00	0.01	0.22	0.04	0.00	0.01	0.01	0.01	0.00	0.00	0.00	99.82
99–08A1	7	%	99.67	0.04	0.04	0.17	0.00	0.00	0.03	0.03	0.00	0.00	0.00	0.01	99.99
99–08A5	31	%	100.53	0.02	0.04	0.29	0.01	0.00	0.00	0.00	0.02	0.00	0.12	0.03	101.06
99–08A5	32	%	100.19	0.00	0.03	0.27	0.04	0.00	0.02	0.01	0.00	0.00	0.00	0.00	100.55
99–08A5	33	%	99.91	0.05	0.02	0.20	0.01	0.00	0.01	0.00	0.01	0.00	0.07	0.01	100.30
99–08A3	40	%	100.08	0.00	0.07	0.30	0.00	0.00	0.02	0.05	0.04	0.05	0.00	0.02	100.63
99–08A3	41	%	99.43	0.00	0.25	0.37	0.05	0.01	0.01	0.01	0.11	0.00	0.05	0.00	100.29
99–08A3	42	%	99.89	0.02	0.24	0.45	0.00	0.01	0.01	0.01	0.07	0.00	0.00	0.00	100.70
99–06C1	45	%	98.97	0.02	0.17	0.16	0.01	0.00	0.02	0.07	0.02	0.01	0.00	0.01	99.47
99–06C1	46	%	99.59	0.01	0.02	0.10	0.00	0.01	0.03	0.00	0.03	0.03	0.12	0.01	99.95
99–03A2	71	%	99.44	0.00	0.08	0.43	0.03	0.00	0.06	0.02	0.06	0.01	0.00	0.00	100.14
99–03A2	72	%	99.54	0.02	0.06	0.25	0.01	0.00	0.05	0.01	0.05	0.00	0.03	0.00	100.04
99–03A4	77	%	99.81	0.00	0.05	0.15	0.01	0.00	0.00	0.09	0.02	0.00	0.03	0.00	100.16
99–03A4	78	%	99.70	0.00	0.31	0.26	0.00	0.02	0.02	0.05	0.16	0.06	0.06	0.05	100.70
99–03A5	83	%	97.83	0.45	0.19	0.78	0.01	0.01	0.01	0.04	0.09	0.03	0.00	0.01	99.44
99–03A5	84	%	99.12	0.03	0.27	0.22	0.03	0.01	0.07	0.03	0.12	0.08	0.00	0.00	99.98
99–03A6	89	%	99.27	0.01	0.28	0.17	0.05	0.03	0.04	0.06	0.15	0.01	0.00	0.02	100.09
99–03A6	90	%	99.30	0.00	0.00	0.05	0.00	0.00	0.04	0.01	0.01	0.06	0.13	0.01	99.60
average	0	%	98.20	0.02	0.35	0.28	0.01	0.03	0.10	0.04	0.17	0.03	0.03	0.01	99.27
Ideal	0	%	100.00	.0	.0	.0	.0	.0	.0	.0	.0	.0	.0	.0	100.00

Table B10. Composition of glass matrix – high iron.

Sample	spot	wt	SiO_2	TiO_2	Al_2O_3	FeO	MnO	MgO	CaO	Na_2O	K_2O	P_2O_5	BaO	Cr_2O_3	Total
97–07A6	50	%	47.51	2.95	8.85	18.90	0.40	3.08	11.61	0.41	2.57	0.77	0.00	0.00	97.05
97–07A6	51	%	47.40	3.12	7.41	15.15	0.36	5.72	15.84	0.19	1.56	0.43	0.00	0.00	97.19
99–10C1	59	%	51.13	3.02	13.30	14.83	0.24	2.81	8.67	0.91	2.36	0.13	0.00	0.01	97.41
99–10C1	60	%	50.26	2.91	11.85	15.38	0.23	4.79	8.93	0.70	2.02	0.16	0.00	0.32	97.55
99–10C2	63	%	50.22	3.11	13.39	18.58	0.24	0.76	8.88	0.79	2.05	0.11	0.00	0.00	98.14
99–10C2	64	%	50.59	2.78	13.72	16.50	0.15	1.17	8.39	0.90	2.29	0.23	0.00	0.00	96.72
99–10C3	69	%	47.66	3.08	11.74	22.28	0.31	1.73	8.18	0.65	1.63	0.18	0.00	0.00	97.44
99–10C5	75	%	48.84	3.04	11.19	17.30	0.30	4.37	9.10	0.65	1.81	0.13	0.00	0.35	97.08
99–10C5	76	%	51.27	2.14	13.03	17.33	0.21	1.70	8.43	0.90	2.04	0.15	0.00	0.00	97.20
99–10C6	79	%	52.59	1.84	12.45	16.08	0.23	2.92	9.40	0.80	2.14	0.17	0.00	0.00	98.63
99–10C6	80	%	48.73	3.22	11.99	18.79	0.30	2.29	9.84	0.64	1.68	0.17	0.00	0.00	97.65
99–10C6	81	%	49.35	4.07	11.71	19.44	0.23	2.03	7.71	0.55	2.03	0.09	0.00	0.26	97.46
99–10C6	82	%	48.78	3.76	10.84	17.95	0.32	4.46	9.03	0.53	1.74	0.14	0.00	0.54	98.10
99–10A1	68	%	47.38	4.36	11.29	20.44	0.41	1.59	9.78	1.23	1.39	0.15	0.18	0.10	98.29
99–10A1	69	%	47.91	4.14	11.69	17.36	0.40	2.47	11.59	1.14	1.48	0.21	0.16	0.13	98.67
99–10A2	72	%	45.61	3.13	10.41	22.94	0.43	2.06	10.48	0.87	1.75	0.16	0.13	0.08	98.05
99–10A2	73	%	45.94	2.65	11.17	21.76	0.41	2.32	11.71	0.84	1.62	0.23	0.17	0.11	98.94
99–10A4	85	%	46.10	3.13	10.43	19.84	0.41	3.17	12.73	0.50	2.02	0.27	0.17	0.07	98.84
99–10A4	86	%	46.08	2.64	10.31	20.49	0.41	3.13	12.35	0.51	2.06	0.23	0.03	0.08	98.31
99–10A6	98	%	46.87	3.60	10.95	22.99	0.49	1.17	8.44	0.82	1.76	0.18	0.18	0.09	97.54
99–10A6	99	%	47.82	4.02	11.15	16.80	0.43	2.92	12.35	0.75	1.81	0.19	0.10	0.14	98.47
99–08A2	14	%	44.54	4.78	14.04	20.77	0.27	0.19	12.22	0.71	1.90	0.45	0.00	0.01	99.85
99–08A2	20	%	44.76	2.41	13.38	23.50	0.34	0.29	11.53	0.65	1.86	0.38	0.00	0.00	99.11
99–08A2	21	%	44.97	4.06	13.45	21.34	0.30	0.23	12.07	0.70	1.77	0.46	0.16	0.00	99.53
99–08A5	37	%	45.25	2.29	10.66	24.57	0.37	2.33	10.85	0.61	1.91	0.31	0.03	0.05	99.24
99–08A5	38	%	45.76	2.72	10.80	23.92	0.38	2.11	11.12	0.73	1.98	0.32	0.00	0.02	99.85
99–08A5	39	%	50.00	1.68	12.36	19.85	0.27	1.16	9.92	1.02	2.75	0.27	0.19	0.02	99.50
99–08A5	38	%	44.81	2.39	10.78	27.82	0.34	1.05	9.45	0.73	1.98	0.31	0.10	0.03	99.81
99–08A5	39	%	49.63	1.62	12.27	19.89	0.33	1.13	9.98	0.99	2.61	0.23	0.12	0.00	98.79
99–08A3	45	%	47.19	4.70	10.39	22.92	0.34	1.67	10.14	0.83	2.14	0.20	0.00	0.03	100.54
99–08A3	46	%	48.12	2.97	12.18	20.95	0.35	0.56	11.44	0.78	1.88	0.37	0.09	0.03	99.72
99–04C3	19	%	42.38	5.20	13.99	23.34	0.25	1.57	8.13	0.66	3.86	0.25	0.00	0.04	99.67
99–04C4	23	%	37.23	2.41	7.74	39.52	0.49	5.07	4.64	0.42	2.25	0.20	0.04	0.00	100.01
99–04C4	26	%	39.26	1.41	9.21	34.88	0.50	3.91	6.58	0.46	2.49	0.23	0.17	0.04	99.13
99–04C4	27	%	42.99	4.11	13.53	23.78	0.29	1.25	10.11	0.58	3.65	0.28	0.15	0.02	100.74
99–04C4	28	%	39.52	5.89	11.92	26.80	0.31	1.21	10.55	0.52	2.64	0.22	0.40	0.02	99.99
99–04C4	29	%	42.33	2.22	11.87	29.04	0.36	2.27	8.74	0.54	2.72	0.24	0.16	0.02	100.52
99–04C2	42	%	43.12	4.62	13.86	22.56	0.24	0.90	11.40	0.52	3.10	0.27	0.16	0.00	100.74
99–04C2	43	%	45.34	2.69	14.54	21.52	0.28	0.54	11.57	0.57	3.44	0.30	0.19	0.00	100.99
99–04C2	44	%	45.46	3.65	16.21	15.35	0.25	0.67	13.45	0.54	3.54	0.25	0.24	0.04	99.65
99–03A1	62	%	46.16	5.76	11.13	15.33	1.28	0.45	16.97	1.90	1.59	0.47	0.03	0.04	101.11
99–03A1	68	%	45.56	4.29	12.95	13.70	1.21	0.22	16.41	1.91	2.73	0.34	0.00	0.09	99.40
99–03A1	69	%	44.92	4.83	12.68	15.52	1.05	0.85	15.04	1.68	3.19	0.36	0.01	0.06	100.19
Average	0	%	46.45	3.34	11.83	20.88	0.39	2.01	10.60	0.78	2.23	0.26	0.08	0.07	98.90

Table B11. Composition of glass matrix - low iron.

Sample	spot	wt	SiO_2	TiO_2	Al_2O_3	FeO	MnO	MgO	CaO	Na_2O	K_2O	P_2O_5	BaO	Cr_2O_3	Total
99–09B2	16	%	55.97	8.52	10.95	5.89	0.35	0.30	8.03	1.39	6.16	0.17	0.31	0.05	98.11
99–10B2	40	%	51.54	4.27	11.87	9.39	0.43	3.47	13.43	0.66	1.97	0.07	0.17	0.32	97.58
99–03B2	44	%	62.19	4.73	11.74	2.19	0.34	1.99	7.99	0.56	4.82	0.07	0.06	0.27	96.95
99–03B2	45	%	61.02	5.14	11.81	3.54	0.32	1.46	6.45	0.82	5.83	0.02	0.20	0.19	96.79
99–04B1	2	%	51.26	5.03	13.14	8.72	0.51	4.22	12.61	0.58	1.91	0.12	0.10	0.29	98.48
99–04B2	4	%	50.44	2.11	22.12	4.92	0.21	1.94	14.31	1.85	0.91	0.07	0.33	0.14	99.35
99–04B2	5	%	50.15	4.58	13.04	9.61	0.52	4.48	12.62	0.63	1.75	0.06	0.00	0.36	97.81
99–04B2	6	%	51.36	4.74	14.07	8.12	0.41	4.94	13.39	1.36	1.47	0.12	0.24	0.41	100.62
99–04B2	8	%	50.30	4.42	12.68	9.83	0.53	4.88	12.83	0.67	1.74	0.13	0.00	0.33	98.33
99–04B2	9	%	49.99	4.69	12.74	10.56	0.51	4.41	12.62	0.69	1.65	0.08	0.00	0.36	98.29
99–04B2	10	%	50.79	4.94	13.08	9.43	0.52	4.31	12.71	0.72	1.81	0.13	0.02	0.31	98.78
99–04B2	11	%	50.12	4.25	13.09	9.77	0.46	4.64	12.78	0.63	1.78	0.09	0.02	0.34	97.95
99–04B2	12	%	50.15	4.41	13.17	9.84	0.50	4.61	12.67	0.67	1.83	0.10	0.15	0.32	98.41
99–09C1	47	%	52.82	5.57	13.66	10.38	0.50	2.73	9.31	0.65	1.79	0.01	0.00	0.42	97.84
99–09C1	48	%	54.37	5.87	13.95	9.95	0.47	2.44	8.89	0.62	1.94	0.00	0.09	0.37	98.96
99–09C1	49	%	53.71	6.22	13.70	10.27	0.57	2.42	9.19	0.62	1.82	0.05	0.06	0.47	99.11
99–09C2	51	%	53.09	5.90	13.75	10.11	0.49	2.98	9.44	0.58	1.77	0.05	0.10	0.43	98.69
99–09C2	52	%	54.61	6.10	13.81	9.77	0.45	2.67	9.26	0.58	1.84	0.06	0.00	0.37	99.54
99–03A1	61	%	51.49	1.67	24.30	2.86	0.32	0.85	13.41	3.01	2.05	0.10	0.08	0.10	100.23
99–03A1	64	%	48.30	5.07	13.58	8.99	0.56	2.98	14.66	1.83	3.27	0.28	0.10	0.19	99.81
99–03A1	65	%	47.24	5.61	13.85	9.78	0.64	2.61	15.23	1.74	3.14	0.43	0.00	0.16	100.43
99–04A1	100	%	46.25	3.54	17.63	10.06	1.06	2.94	10.78	0.74	3.73	0.06	0.34	0.00	97.13
99–04A1	101	%	46.99	3.39	18.32	10.16	1.01	2.12	9.98	0.78	4.23	0.12	0.26	0.00	97.35
99–04A3	107	%	47.08	3.30	17.00	9.09	1.14	3.74	11.99	0.72	3.24	0.14	0.29	0.00	97.73
99–04A3	108	%	46.77	3.44	16.61	7.09	0.77	5.32	14.28	0.61	3.23	0.22	0.23	0.00	98.57
Average	0	%	51.52	4.70	14.55	8.41	0.54	3.18	11.55	0.95	2.63	0.11	0.13	0.25	98.51

Table B12. Composition of glass matrix – high lime.

Sample	spot	wt	SiO_2	TiO_2	Al_2O_3	FeO	MnO	MgO	CaO	Na_2O	K_2O	P_2O_5	BaO	Cr_2O_3	Total
99–10B1	36	%	51.28	4.26	12.35	8.76	0.52	3.29	14.48	0.65	1.97	0.06	0.23	0.31	98.16
99–10B1	37	%	52.26	4.39	12.41	7.91	0.47	2.85	13.89	0.68	2.25	0.08	0.19	0.32	97.69
99–10B2	41	%	52.52	4.34	12.18	7.53	0.48	2.93	14.13	0.67	2.08	0.07	0.08	0.32	97.33
99–04B3	13	%	53.95	6.41	13.87	4.37	0.62	3.27	13.97	0.15	1.75	0.00	0.00	0.34	98.69
99–04B3	14	%	54.11	6.05	13.63	4.00	0.58	3.33	14.08	0.18	1.78	0.00	0.00	0.31	98.05
99–04B3	15	%	54.07	6.24	13.55	3.81	0.54	3.44	14.49	0.14	1.76	0.03	0.06	0.33	98.44
99–03A1	63	%	46.51	6.16	11.42	11.78	0.82	2.57	15.94	1.28	2.25	0.29	0.00	0.19	99.21
99–03A1	66	%	46.62	5.24	13.56	10.26	0.62	2.86	15.90	1.58	3.19	0.35	0.00	0.18	100.37
99–03A1	67	%	45.03	5.23	12.93	9.36	0.58	4.16	17.78	1.14	2.41	0.37	0.07	0.33	99.40
99–03A1	70	%	44.26	4.88	10.14	14.12	0.77	2.71	18.91	0.94	1.92	0.35	0.07	0.12	99.20
99–03A4	80	%	53.70	4.60	11.90	6.23	0.41	2.00	17.45	1.05	1.31	0.09	0.04	0.04	98.83
99–03A4	82	%	54.34	3.45	12.71	5.21	0.62	1.95	16.85	1.13	2.01	0.16	0.16	0.33	98.92
99–03A5	85	%	53.81	3.60	12.32	5.76	0.56	1.86	17.12	1.10	1.80	0.11	0.20	0.10	98.33
99–03A5	87	%	53.05	3.54	11.38	5.73	0.76	2.12	19.81	1.00	1.24	0.17	0.01	0.16	98.98
99–03A6	91	%	51.47	4.10	12.91	5.30	0.59	1.90	19.39	1.40	2.43	0.23	0.00	0.03	99.76
99–04A3	110	%	49.23	2.96	19.70	6.75	1.02	1.66	10.55	0.92	4.46	0.17	0.31	0.01	97.72
Average	0	%	51.01	4.72	12.94	7.31	0.62	2.68	15.92	0.88	2.16	0.16	0.09	0.21	98.69

Table B13. Composition of glass matrix – high potash and low lime - leucite normative

Sample	spot	wt	SiO_2	TiO_2	Al_2O_3	FeO	MnO	MgO	CaO	Na_2O	K_2O	P_2O_5	BaO	Cr_2O_3	Total
97–07A1	23	%	56.86	3.97	14.94	7.51	0.23	0.54	4.85	1.47	6.87	0.54	0.00	0.00	97.79
97–07A1	24	%	55.51	5.31	13.55	8.94	0.45	0.74	5.03	1.28	6.34	0.39	0.00	0.00	97.54
97–07A1	25	%	56.01	5.25	13.14	7.83	0.42	0.79	5.74	1.21	6.14	0.33	0.00	0.00	96.85
97–07A7	56	%	59.06	1.66	14.50	6.93	0.48	0.79	7.26	0.75	4.68	0.54	0.00	0.00	96.64
99–06B2	16	%	55.97	8.52	10.95	5.89	0.35	0.30	8.03	1.39	6.16	0.17	0.31	0.05	98.11
99–06B2	17	%	61.05	4.64	12.61	5.23	0.38	0.45	5.26	1.56	6.97	0.20	0.12	0.01	98.48
99–03B2	44	%	62.19	4.73	11.74	2.19	0.34	1.99	7.99	0.56	4.82	0.07	0.06	0.27	96.95
99–03B2	45	%	61.02	5.14	11.81	3.54	0.32	1.46	6.45	0.82	5.83	0.02	0.20	0.19	96.79
Average	0	%	58.46	4.90	12.91	6.01	0.37	0.88	6.33	1.13	5.98	0.28	0.09	0.07	97.39

Table B14. Composition of glass matrix – low lime, high iron - hercynite normative.

Sample	spot	wt	SiO_2	TiO_2	Al_2O_3	FeO	MnO	MgO	CaO	Na_2O	K_2O	P_2O_5	BaO	Cr_2O_3	Total
99–10C3	70	%	50.93	2.79	13.49	18.66	0.15	0.90	7.19	0.86	2.40	0.21	0.00	0.00	97.56
99–08A1	8	%	50.77	3.48	10.90	24.26	0.93	1.28	4.74	0.97	1.78	0.35	0.09	0.05	99.60
99–08A1	10	%	52.41	4.05	12.06	23.53	0.94	0.85	2.62	0.86	1.62	0.39	0.00	0.01	99.34
99–08A4	28	%	45.89	4.31	14.38	28.47	0.51	0.24	2.97	0.52	1.81	0.34	0.07	0.03	99.54
99–08A4	29	%	48.06	1.67	14.76	26.35	0.54	0.27	4.24	0.56	1.44	0.44	0.00	0.03	98.35
99–08A4	30	%	47.79	1.53	14.00	28.46	0.57	0.35	3.24	0.64	1.33	0.34	0.05	0.00	98.32
Average	0	%	49.30	2.97	13.26	24.96	0.61	0.64	4.17	0.74	1.73	0.35	0.04	0.02	98.79

Table B15. Composition of glass matrix – low lime, low iron - mullite normative.

Sample	spot	wt	SiO_2	TiO_2	Al_2O_3	FeO	MnO	MgO	CaO	Na_2O	K_2O	P_2O_5	BaO	Cr_2O_3	Total
99–10C1	57	%	54.95	0.94	29.42	2.54	0.00	0.34	1.98	1.33	5.47	0.02	0.00	0.00	96.99
99–10C1	58	%	59.58	0.83	19.39	4.21	0.00	0.60	3.29	1.71	6.26	0.08	0.00	0.00	95.94
99–03A4	81	%	65.80	0.04	19.78	0.84	0.08	0.94	3.04	2.59	6.54	0.09	0.00	0.04	99.77
99–03A4	79	%	57.81	0.01	25.01	1.01	0.04	0.65	10.50	2.62	2.00	0.04	0.07	0.11	99.87
Average	0	%	59.54	0.46	23.40	2.15	0.03	0.63	4.70	2.06	5.07	0.06	0.02	0.04	98.14